AGU PUBLICATIONS

Paleoceanography

RESEARCH ARTICLE
10.1002/2014PA002687

Key Points:
- Coiling ratio of G. truncatulinoides indicative of depth of the thermocline
- Single-specimen isotopes of G. truncatulinoides confirm inferred depth habitat

Correspondence to:
W. Feldmeijer,
w.feldmeijer@vu.nl

Citation:
Feldmeijer, W., B. Metcalfe, G.-J. A. Brummer, and G. M. Ganssen (2015), Reconstructing the depth of the permanent thermocline through the morphology and geochemistry of the deep dwelling planktonic foraminifer *Globorotalia truncatulinoides*, *Paleoceanography*, *30*, 1–22, doi:10.1002/2014PA002687.

Received 20 JUN 2014
Accepted 15 DEC 2014
Accepted article online 17 DEC 2014
Published online 23 JAN 2015

Reconstructing the depth of the permanent thermocline through the morphology and geochemistry of the deep dwelling planktonic foraminifer *Globorotalia truncatulinoides*

W. Feldmeijer[1], B. Metcalfe[1], G.-J. A. Brummer[1,2], and G. M. Ganssen[1]

[1]Earth and Climate Cluster, Faculty of Earth and Life Sciences, VU University Amsterdam, Amsterdam, Netherlands, [2]Department of Marine Geology and Chemical Oceanography, NIOZ Royal Netherlands Institute for Sea Research, Den Burg, Netherlands

Abstract Geochemical and morphological characteristics of *Globorotalia truncatulinoides*, a deep dwelling planktonic foraminifer, have been used since the mid-1950s to infer (paleo)oceanographic conditions of the upper ocean. The coiling ratio has been linked to different water masses and stable oxygen isotope signal of this species to changes in depth habitat and/or season. Here we show that the isotopic composition of single specimens covering Termination III of multiple size fractions of North Atlantic *G. truncatulinoides*$_{sinistral}$ is indicative of a deeper calcification depth in the water column compared to *G. truncatulinoides*$_{dextral}$ as previously indirectly inferred in a plankton tow study. Furthermore, the change in coiling ratio from dominantly *G. truncatulinoides*$_{dextral}$ (95%) to brief episodes of dominantly *G. truncatulinoides*$_{sinistral}$ (80%) gives a strong indication of deepening of the permanent thermocline during periods in which *G. truncatulinoides*$_{sinistral}$ was dominant. The position of the permanent thermocline during marine isotope stages 8 and 7 echoes the relative strength of the Atlantic meridional overturning circulation (AMOC), dominated by interglacial-glacial dynamics. We demonstrate that Glacial Heinrich (ice-rafted debris) events appear to proceed a permanent thermocline shoaling, whereas interglacial Heinrich events follow the shoaling of the permanent thermocline, likely a result of a weakened AMOC.

1. Introduction

Variations in the depth of the permanent thermocline over glacial-interglacial cycles have important implications for understanding the dynamics of the upper ocean during climate change. Through wind, waves, and convective action, the heating of the ocean surface caused by solar radiation can be mixed deeper into the water column. Given the specific heat capacity of oceanic water, this surface mixed layer has a strong implication for the storage of heat. These upper homogenous waters, with nearly uniform properties (i.e., temperature and salinity), are separated from deeper water by a layer with a rapid temperature change situated (in the North Atlantic) around 200–1000 m water depth [*Pinet*, 2009], called the permanent thermocline. The permanent thermocline is also defined as the depth with the largest vertical temperature gradient. At higher latitudes where the influx of solar radiation differs seasonally, a secondary seasonal thermocline can form in response to reduced turbidity and increase insolation at a depth above the permanent thermocline. As *Globorotalia truncatulinoides* [*d'Orbigny* 1839] calcifies down to depths close to the permanent thermocline, this is an ideal species to investigate fluctuations in the depth of the permanent thermocline.

Globally, the first synchronous appearance of *G. truncatulinoides* occurs and marks the base of the Pliocene-Pleistocene boundary (approximately 2.0 Ma, below the Olduvai Subchron) [*Hays and Berggren*, 1971]. However, the species originates much earlier at 2.82 Ma (during the Gauss magnetochron) [*Dowsett*, 1989; *Lazarus et al*., 1995; *Spencer-Cervato and Thierstein*, 1997] in the Southwest Pacific, immigrating 600 kyr later into the Indian Ocean at 2.2 Ma and into the Atlantic Ocean at around 2.1 Ma. However, *Sexton and Norris* [2008] used high-resolution abundance counts with a temporal resolution of 3 kyr and note an earlier 19 kyr invasion of the early SW Pacific forms, similar to the modern subtropical morphotypes, into the Atlantic 200 kyr after its evolution at 2.544–2.525 Ma, with the later semipermanent colonization of the Atlantic Ocean occurring at 2.03 Ma [*Spencer-Cervato and Thierstein*, 1997]. *Globorotalia truncatulinoides*, being the evolutionary youngest member of the modern planktonic foraminiferal assemblage [*Spencer-Cervato and Thierstein*, 1997], is deep

dwelling and is thought to reproduce at ~600 m. Juveniles subsequently traveling back to surface waters wherein to slowly sink down the water column during ontogeny [*Bé*, 1977; *Bé et al*., 1985; *Hemleben et al*., 1989; *Kemle-von Mücke and Hemleben*, 1999; *Vergnaud-Grazzini*, 1976] calcifying down to water depths of ~1000 m [*Bé*, 1960; *Durazzi*, 1981; *Hemleben et al*., 1985, 1989; *Lohmann and Schweitzer*, 1990]. Thus, this species is considered to record local hydrography down to the depth of the permanent thermocline [*LeGrande et al*., 2004; *Lohmann and Schweitzer*, 1990; *Martínez*, 1994, 1997; *Ravelo and Fairbanks*, 1992; *Steph et al*., 2009], and many researchers utilize the species as a proxy for subsurface paleoceanographic conditions [*Cléroux et al*., 2007; *Erez and Honjo*, 1981; *Healy-Williams et al*., 1985; *Kennett*, 1968; *Lohmann*, 1992; *Lohmann and Malmgren*, 1983; *Lohmann and Schweitzer*, 1990; *Martínez*, 1994, 1997; *Mulitza et al*., 1997; *Pharr and Williams*, 1987].

Furthermore, the coiling direction of *G. truncatulinoides* appears linked to depth habitat [*Lohmann*, 1992], different water masses [*Bé*, 1960; *Ericson et al*., 1955; *Thiede*, 1971; *Tolderlund and Be*, 1971], and/or seasons [*Lončarić et al*., 2005, 2007]. Left and right coiling of chamber arrangement is exhibited within numerous members of the modern planktonic foraminiferal species [*Brummer and Kroon*, 1988], but a clear species distinction between sinistral and dextral is only apparent in a few species, e.g., *Neogloboquadrina pachyderma* and *G. truncatulinoides*. Furthermore, this morphological characteristic has been shown as a discernable characteristic of genetic variance in but a few species [*Darling et al*., 1997]. Coiling ratios have however been shown to indicate a change in environment and therefore make an ideal quantitative biomarker in the fossil record. The ratios of sinistral and dextral *G. truncatulinoides* were first utilized as an environmental tracer by *Ericson et al*. [1955], following on from the suggestion of an evolutionary significance [*Bolli*, 1950, 1951], who went on to determine a core-top coiling ratio provenance relationship. Further analysis of *G. truncatulinoides* has revealed both a complex morphological appearance and genetic variance within the species [*de Vargas et al*., 2001; *Renaud and Schmidt*, 2003]. *de Vargas et al*. [2001] found, through analysis of subunit ribonucleic acid ribosomal genes, that there exist four genotypes associated with the modern taxonomic unit with each genetically distinct species being adapted to different hydrographic conditions. *de Vargas et al*. [2001] defined morphological characteristics that allowed some distinction to be made; using this, *Renaud and Schmidt* [2003] found that these four cryptic species of *G. truncatulinoides* follow downcore temperature variations for the past 140 kyr. Later, it was *Ujiié and Lipps* [2009] who added a fifth genotype, and as the study by *de Vargas et al*. [2001] did not perform genetic and morphological analysis on the same specimens, *Quillévéré et al*. [2013] did a more elaborate and global study on the morphological characteristics of *G. truncatulinoides*.

Given that modern specimens of *G. truncatulinoides* have a depth habitat that covers, in some regions, the upper 1000 m of the water column [*Hemleben et al*., 1985], the environmental conditions that control the species distribution are difficult to distinguish, given the variability in terms of temperature, salinity, mixing, turbulence, productivity and associated nutrients, and prey abundance [*Hemleben et al*., 1989; *Kemle-von Mücke and Hemleben*, 1999]. Sediment trap data of *G. truncatulinoides* from various regions indicate fluxes from winter until spring [*Deuser and Ross*, 1989; *Deuser et al*., 1981; *Eguchi et al*., 1999; *Storz et al*., 2009; *Vergnaud-Grazzini*, 1976; *Wilke et al*., 2009], although it has been suggested that this species has a potential life span of 1 year [*Hemleben et al*., 1989]. Longevity combined with its relatively large depth habitat would suggest that *G. truncatulinoides* is severely prone to expatriation, yet the geographic distribution patterns from both sediment and plankton studies are analogous [*de Vargas et al*., 2001; *Healy-Williams and Williams*, 1981; *Kennett*, 1968; *Lohmann and Malmgren*, 1983]. The findings in the aforementioned studies and the selection of a single morphotype (see section 2) will reduce the risk of analyzing multiple, laterally transported genetic species of *G. truncatulinoides* [*Renaud and Schmidt*, 2003] as our core is located close to an east-west morphospecies boundary and the North Atlantic gyre would transport a different morphospecies toward the core area.

Based on plankton tows, *Lohmann and Schweitzer* [1990] hypothesized that *G. truncatulinoides*$_{\text{sinistral}}$ has a deeper preferred habitat in the water column than *G. truncatulinoides*$_{\text{dextral}}$. Plankton tow samples, from the same area of our study [*Ottens*, 1992], confirm this, finding large concentration of *G. truncatulinoides*$_{\text{sinistral}}$ deeper in the water column (700–800 m water depth) compared to concentrations of *G. truncatulinoides*$_{\text{dextral}}$ closer to the surface (400–500 m water depth). Analysis of both the coiling ratio and the stable isotope composition of different size fractions of *G. truncatulinoides* across Termination III, presented here, reveals that a similar ecological structuring occurred 200–260 kyr before present. Marine isotope stages 8 and 7 are important periods of habitat expansion of *G. truncatulinoides*; it was during this period that the species

underwent two southward expansions of its habitat into (sub)Antarctic waters at ~200 and ~300 kyr [*Kennett*, 1970; *Pharr and Williams*, 1987]. Paleoceanographically, Termination III is an under studied period in recent Earth history, despite its great similarity to the stepwise warming of the most recent Termination I (i.e., Younger Dryas [*Cheng et al*., 2009]) and having the strongest precession, obliquity, and eccentricity forcing, driving the Northern Hemisphere solar insolation, of the past 500 kyr [*Ruddiman*, 2001]. Thus, this time period is expected to show the strongest seasonal variability; however, it poses a conundrum in having been the least pronounced glaciation. In more recent years, research has focused on the role of the ocean in providing the feedback necessary for initiation of glaciation and the abruptness of deglaciations. Reconstruction of the depth of the permanent thermocline enables a look at the heat distribution within the ocean. Analyzing the range in oxygen isotopes for multiple individuals within one sample will give an indication of either seasonal temperature variability or depth habitat dominating their observed chemistry [*Ganssen et al*., 2011; *Killingley et al*., 1981]. As the seasonal temperature variability is ~1–2°C at the preferred depth habitat of *G. truncatulinoides* [*Levitus*, 2009], the range will mainly reflect depth migration. Therefore, this study will give new insights into the viability of using *G. truncatulinoides* as a proxy for past changes in the depth of the permanent thermocline.

2. Methodology

Samples from North Atlantic piston core Joint Global Ocean Flux Study Actuomicropaleontology Paleoceanography North Atlantic Project T90-9P (45°17.5′N, 27°41.3′W; 2934 m water depth; core length = 1028 cm) were taken from depth interval 728–828 cm, with 1 cm slices taken at 4 cm intervals across marine isotope stages (MISs) 8 and 7 including Termination III, representing the period between about 260 and 200 kyr including Heinrich events (HEs) 15 and 14 (Figure 1) [*Lototskaya et al*., 1998]. Washed samples were size fractionated by dry sieving into 212–250 μm, 250–300 μm, 300–355 μm, and 355–400 μm intervals. The coiling ratio between dextral and sinistral *G. truncatulinoides* (Figure 2) for individual size fractions was based upon counts of 100 specimens.

From the subsequent size fractions, where possible, 20 specimens of *G. truncatulinoides*$_{\text{dextral}}$ were picked following the taxonomy of *Bé* [1977] for single-specimen isotopic analysis. As there are multiple (genetic) species of *G. truncatulinoides* [*de Vargas et al*., 2001; *Quillévéré et al*., 2011; *Ujiié and Lipps*, 2009; *Ujiié and Asami*, 2013; *Ujiié et al*., 2010], all specimens were picked and counted following the morphotypes depicted in Figure 2. We assume, based upon a visual comparison, that we have analyzed species II as defined by *de Vargas et al*. [2001]. This assumption is further strengthened by the findings of *Ujiié et al*. [2010], only seeing both coiling varieties in species II. At present, little is known about the metabolic, or calcification, processes associated with each genetic species, and therefore, the "vital effect," or deviation from equilibrium, is not known. However, it is likely that as the genetoypes have similar morphology (including encrustment) and come from the same lineage that the underlying process of calcification can be assumed to be the same or at least had not drastically altered. Furthermore, the study by *Lončarić et al*. [2006] found no deviation from δ^{18}O equilibrium in *G. truncatulinoides* from the South Atlantic. As opposed to oxygen isotopes, which reflect the ambient hydrology at the time of calcification, deviation in carbon isotopes between genotypes may be apparent due to underlying diversification of niches (i.e., different prey).

Samples were analyzed on a Thermo Finnigan Delta^{+} mass spectrometer equipped with a GasBench II preparation device. Samples were placed in a He-filled 3 mL exetainer vial and digested in concentrated H_3PO_4 at a temperature of 45°C. Subsequently, the CO_2-He gas mixture is transported to the GasBench II by the use of a He flow through a flushing needle system where water is extracted from the gas using a Nafion tubing. CO_2 is analyzed in the mass spectrometer after separation of other gases in a gas chromatography column. Isotope values are reported as the standard denotation δ^{13}C and δ^{18}O in per mil versus Vienna Peedee belemnite. Reproducibility of routinely analyzed laboratory $CaCO_3$ standards is within 0.1‰ (1σ) for both δ^{18}O and δ^{13}C.

Each data set for the discrete depth intervals was tested for normality using a Shapiro-Wilk test; those samples that deviated from normality ($p < 0.05$) were separated into two distributions using the mixture analysis in PAST [*Hammer et al*., 2001]. The corresponding unmixed distributions were evaluated using the Akaike information criterion, where minimal values indicate that the grouping chosen does not overfit the data. The test of *Ashman et al*. [1994] for quantifying bimodality was performed to determine whether there is a clear separation into two modes ($D > 2$); these results are reported in Table 1. In order to determine whether a change in stratification, i.e., a change in the depth of the permanent thermocline, occurs, samples were

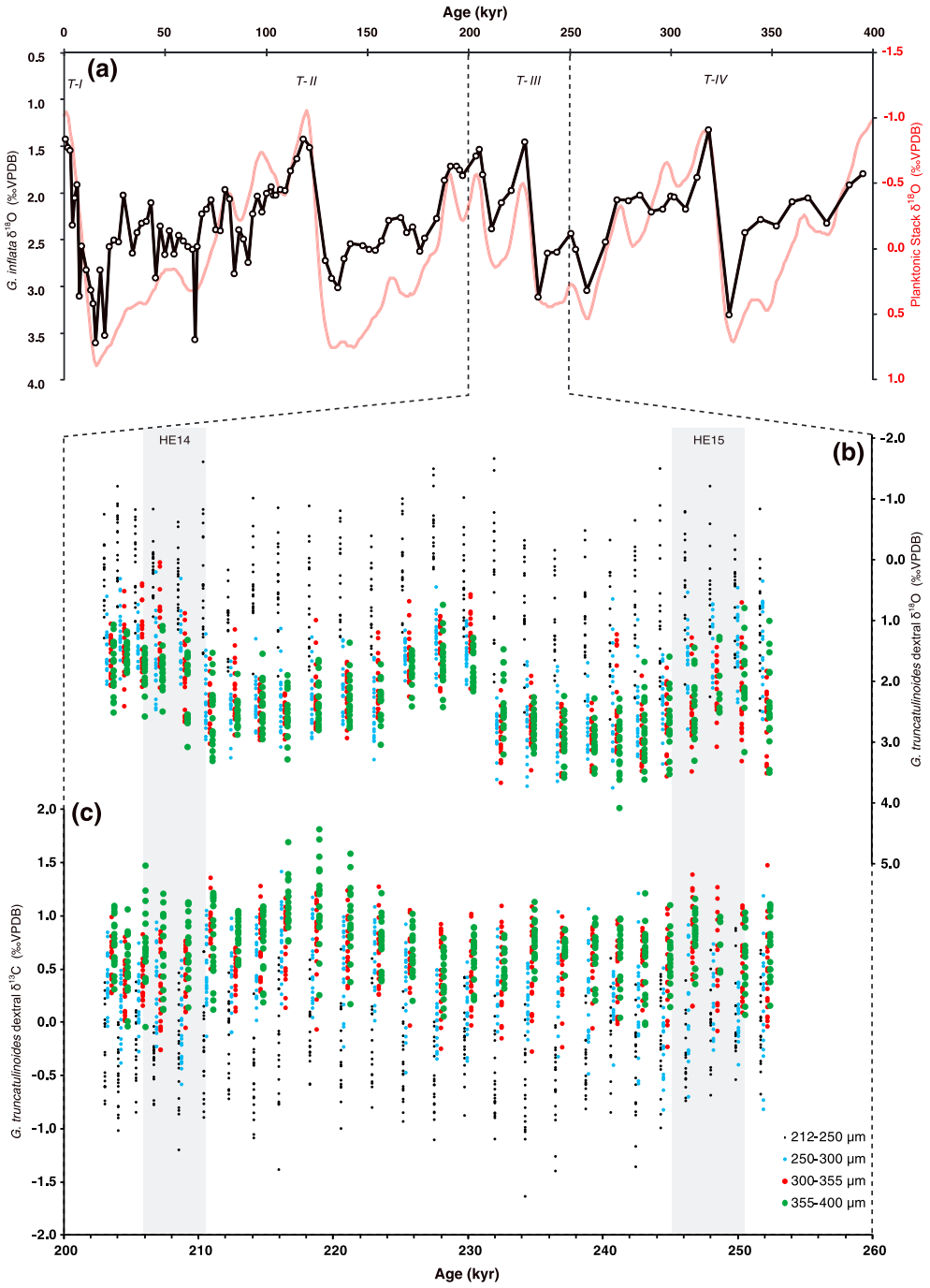

Figure 1. (a) Planktonic foraminiferal stratigraphy of core T90-9P from *Lototskaya et al.* [1998] based on 30–50 specimens of *Globorotalia inflata* compared to the planktonic stack of *Huybers* [2007] in red and single-specimen (b) δ^{18}O and (c) δ^{13}C data for *G. truncatulinoides*$_{\text{dextral}}$ of four size fractions 212–250 µm (black), 250–300 µm (blue), 300–355 µm (red), and 355–400 µm (green). Outlier correction based on interquartile range (IQR): $Q_1 - 1.5 \cdot \text{IQR}$ and $Q_3 + 1.5 \cdot \text{IQR}$. Note that single-specimen data from four size fractions of the same sample have been offset on the horizontal axis for clarification reasons. Heinrich layers 14 and 15, based on IRD abundance (Feldmeijer et al., in preparation), are indicated with grey bars.

tested, using an *F* test and subsequently a *t* test for independent samples (or Welch test, depending on the *F* value) to see whether (i) the means between size fractions of the same coiling direction are different (Table 1) and (ii) the means between coiling directions of the same size fraction are different (Table 2). Subsequently, all samples were tested for covariance between oxygen and carbon isotopes of individuals from the same

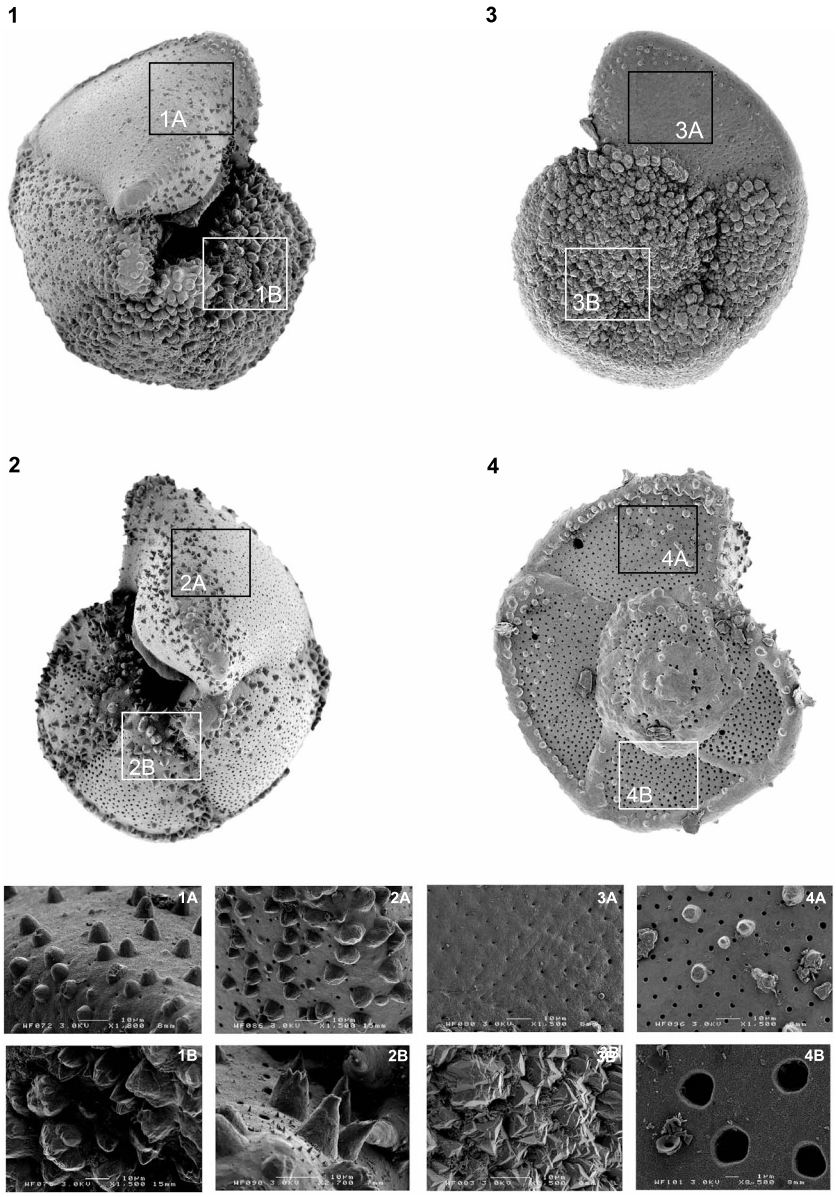

Figure 2. Scanning electron microscope pictures of *G. truncatulinoides*$_{\text{sinistral}}$ (1 and 3) and *G. truncatulinoides*$_{\text{dextral}}$ (2 and 4) showing various levels of encrustation from specimens and chambers with no encrustation (3A and 4A) to heavily encrusted (1B and 3B). Note that even nonencrusted forms have pustules that appear to lie along suture lines and close to the aperture. For illustrative purposes, we have shown specimens with high and low encrustation; however, the level of encrustation is irrespective of coiling direction.

sample (Table 3). These analyses were performed in PAST [*Hammer et al.*, 2001] on individual samples per size fraction and for all four size fractions combined. The correlation coefficient ($-1 < CC < 1$) was calculated by dividing the covariance by the product of the two standard deviations (of the oxygen and carbon isotopes) to have a measure of covariance independent of the sample variance. A CC of -1 would mean a strong negative covariance, a CC of 1 would indicate a strong positive covariance, and a CC of 0 shows no covariance (Table 4).

3. Results and Discussion

3.1. Bioturbation Impact on Proxy Records

Bioturbation, the mechanical mixing of the sediment by benthic organisms, could pose a problem interpreting high-resolution data recovered from the sediment such as that presented here. Assuming

Paleoceanography

10.1002/2014PA002687

Table 1. Statistical Test Values for Testing Whether the Means Between Size Fractions of the Same Coiling Direction Are Different[a]

	Size Fraction						Test for Equal Means				Test for Equal Variance	
Age (kyr)	Lower Limit (μm)	Upper Limit (μm)	Sinistral Mean	Dextral Mean	Sinistral Variance	Dextral Variance	*T* Value	*p* (Same Mean)	Unequal Variance Test	*p* (Same Mean)	*F* Test	*P* (Same Variance)
						Oxygen						
209	355	400	2.380	2.130	0.084	0.291			1.793	0.084	3.455	0.010
211	355	400	2.369	2.525	0.119	0.266	−1.095	0.281			2.234	0.097
216	355	400	2.178	2.562	0.135	0.137	−3.200	0.003			1.013	0.971
241	355	400	2.804	3.057	0.087	0.213	−1.970	0.057			2.441	0.072
243	355	400	2.569	2.790	0.168	0.242	−1.521	0.137			1.438	0.446
247	355	400	2.201	2.474	0.424	0.247	−1.468	0.151			1.714	0.259
209	212	250	1.702	0.401	0.305	0.263	7.636	0.000			1.160	0.750
211	212	250	2.010	0.370	0.257	0.780			7.154	0.000	3.031	0.023
216	212	250	1.628	0.447	0.296	0.450	6.118	0.000			1.520	0.369
241	212	250	2.764	1.176	0.204	0.696			6.853	0.000	3.403	0.013
243	212	250	2.453	0.825	0.616	0.780	5.916	0.000			1.266	0.631
247	212	250	1.854	0.352	0.615	0.624	5.556	0.000			1.015	0.968
						Carbon						
209	355	400	0.729	0.723	0.042	0.095	0.071	0.944			2.275	0.084
211	355	400	0.666	0.799	0.046	0.134			−1.381	0.177	2.887	0.029
216	355	400	0.560	1.106	0.114	0.055	−5.718	0.000			2.081	0.135
241	355	400	0.611	0.707	0.077	0.102	−0.976	0.336			1.324	0.568
243	355	400	0.559	0.593	0.043	0.105	−0.376	0.709			2.468	0.067
247	355	400	0.604	0.799	0.087	0.051	−2.242	0.031			1.700	0.280
209	212	250	−0.043	−0.300	0.134	0.198	1.958	0.058			1.480	0.411
211	212	250	0.009	−0.246	0.202	0.195	1.789	0.082			1.036	0.936
216	212	250	0.090	−0.186	0.132	0.284	1.914	0.063			2.160	0.102
241	212	250	0.064	−0.153	0.152	0.142	1.650	0.108			1.069	0.916
243	212	250	−0.120	−0.406	0.413	0.212	1.578	0.123			1.948	0.167
247	212	250	0.095	−0.314	0.179	0.103	3.194	0.003			1.738	0.282

[a]An *F* test was performed to test for equal variances ($H_0 = {\sigma_1}^2 = {\sigma_2}^2$), samples with the same variance were tested with a *t* test for independent samples, and those that have different variances were tested with a Welch test ($H_0 = {\mu_1}^2 = {\mu_2}^2$). The critical value is $p < 0.05$ for all tests.

Paleoceanography

10.1002/2014PA002687

Table 2. Statistical Test Values for Testing Whether the Means Between Coiling Directions of the Same Size Fraction Are Different[a]

						Test for Equal Means				Test for Equal Variance	
Age (kyr)	Coiling Direction	355–400 μm Mean	212–250 μm Mean	355–400 μm Variance	212–250 μm Variance	*T* Value	*p* (Same Mean)	Unequal Variance Test	*p* (Same Mean)	*F* Test	*p* (Same Variance)
					Oxygen						
209	sinistral	2.380	1.702	0.084	0.305			4.765	>0.001	3.619	0.008
211		2.369	2.010	0.119	0.257	2.555	0.015			2.162	0.111
216		2.178	1.628	0.135	0.296	3.749	0.001			2.185	0.097
241		2.804	2.764	0.087	0.204	0.322	0.749			2.345	0.083
243		2.569	2.453	0.168	0.616			0.557	0.582	3.669	0.009
247		2.201	1.854	0.424	0.615	1.486	0.146			1.452	0.430
209	dextral	2.130	0.401	0.291	0.263	10.266	0.000			1.107	0.825
211		2.525	0.370	0.266	0.780			9.363	>0.001	2.934	0.027
216		2.562	0.447	0.137	0.450			12.192	>0.001	3.278	0.017
241		3.057	1.176	0.213	0.696			8.044	>0.001	3.270	0.019
243		2.790	0.825	0.242	0.780			8.526	>0.001	3.229	0.015
247		2.474	0.352	0.247	0.624	9.665	0.000			2.527	0.063
					Carbon						
209	sinistral	0.729	−0.043	0.042	0.134			8.074	>0.001	3.225	0.015
211		0.666	0.009	0.046	0.202			5.739	>0.001	4.354	0.003
216		0.560	0.090	0.114	0.132	4.236	0.000			1.150	0.763
241		0.611	0.064	0.077	0.152	4.929	0.000			1.971	0.165
243		0.559	−0.120	0.043	0.413			4.374	>0.001	9.716	0.000
247		0.604	0.095	0.087	0.179	4.344	0.000			2.051	0.134
209	dextral	0.723	−0.300	0.095	0.198	8.297	0.000			2.097	0.123
211		0.799	−0.246	0.134	0.195	8.138	0.000			1.455	0.421
216		1.106	−0.186	0.055	0.284			9.830	>0.001	5.170	0.001
241		0.707	−0.153	0.102	0.142	7.198	0.000			1.394	0.501
243		0.593	−0.406	0.105	0.212	7.868	0.000			2.021	0.137
247		0.799	−0.314	0.051	0.103	11.791	0.000			2.006	0.169

[a]An *F* test was performed to test for equal variances ($H_0 = {\sigma_1}^2 = {\sigma_2}^2$), samples with the same variance were tested with a *t* test for independent samples, and those that have different variances were tested with a Welch test ($H_0 = {\mu_1}^2 = {\mu_2}^2$). The critical value is $p < 0.05$ for all tests.

Table 3. Covariance and Correlation Coefficients (CC) Between Oxygen and Carbon Isotopes of Individuals From the Same Sample for All *G. truncatulinoides*$_{dextral}$ and *G. truncatulinoides*$_{sinistral}$[a]

		G. truncatulinoides (Dextral)											
		Covariance				Product of Standard Deviations				Correlation Coefficient			
Depth in Core (cm)	Age (kyr)	212–250 μm	250–300 μm	300–355 μm	355–400 μm	212–250 μm	250–300 μm	300–355 μm	355–400 μm	212–250 μm	250–300 μm	300–355 μm	355–400 μm
729	203.4	0.11	0.06	0.05	0.06	0.19	0.09	0.10	0.10	0.55	0.67	0.54	0.57
732	204.4	0.12	0.05	0.06	0.05	0.18	0.13	0.10	0.10	0.68	0.40	0.59	0.50
736	205.7	0.11	0.03	0.05	0.12	0.22	0.09	0.11	0.15	0.53	0.35	0.50	0.77
740	207.0	0.07	0.11	0.17	0.06	0.13	0.18	0.21	0.12	0.55	0.59	0.83	0.50
744	208.9	0.01	0.12	0.07	0.11	0.24	0.15	0.13	0.16	0.03	0.78	0.51	0.65
748	210.7	0.18	0.10	0.05	0.12	0.39	0.15	0.10	0.23	0.47	0.67	0.49	0.51
752	212.6	0.12	0.10	0.09	0.01	0.22	0.16	0.12	0.04	0.56	0.66	0.71	0.37
756	214.5	0.21	0.09	0.06	0.06	0.34	0.17	0.11	0.11	0.61	0.53	0.55	0.52
760	216.3	0.26	0.08	0.08	0.05	0.30	0.12	0.15	0.14	0.86	0.72	0.55	0.38
764	218.6	0.30	0.08	0.08	0.06	0.35	0.17	0.17	0.17	0.86	0.50	0.51	0.36
768	220.9	0.18	0.10	0.05	0.06	0.31	0.16	0.12	0.12	0.58	0.64	0.40	0.52
772	223.2	0.23	0.08	0.06	0.04	0.30	0.16	0.12	0.10	0.74	0.49	0.51	0.38
776	225.5	0.15	0.08	0.09	0.02	0.20	0.16	0.14	0.08	0.76	0.47	0.62	0.24
780	227.8	0.13	0.04	0.05	0.06	0.23	0.11	0.14	0.12	0.57	0.36	0.38	0.52
784	230.1	0.13	0.05	0.08	0.02	0.22	0.10	0.10	0.06	0.58	0.50	0.83	0.36
788	232.3	0.19	0.04	0.17	−0.01	0.37	0.14	0.33	0.11	0.51	0.26	0.51	−0.08
792	234.6	0.23	0.04	0.03	0.01	0.29	0.13	0.12	0.05	0.80	0.32	0.27	0.10
796	236.8	0.26	0.20	0.05	0.02	0.42	0.23	0.12	0.06	0.63	0.86	0.37	0.37
800	239.1	0.09	0.08	0.05	0.04	0.25	0.16	0.07	0.09	0.36	0.48	0.74	0.47
804	240.9	0.26	0.19	0.10	0.00	0.39	0.35	0.25	0.15	0.68	0.55	0.38	−0.01
808	242.8	0.18	0.15	−0.01	−0.01	0.39	0.28	0.10	0.17	0.45	0.52	−0.11	−0.05
812	244.6	0.28	0.07	0.09	0.04	0.51	0.14	0.20	0.12	0.55	0.46	0.43	0.37
816	246.5	0.15	0.14	0.09	0.01	0.25	0.26	0.20	0.16	0.58	0.54	0.46	0.07
820	248.4	0.15	0.12	0.08	0.09	0.30	0.17	0.23	0.18	0.51	0.69	0.35	0.50
824	250.2	0.13	0.02	0.06	0.05	0.38	0.16	0.24	0.17	0.33	0.12	0.24	0.30
828	252.1	−0.09	0.11	0.06	0.06	0.30	0.38	0.20	0.20	−0.30	0.29	0.32	0.33
									Average	0.54	0.52	048	0.37

that bioturbation would generate two (or more) populations within a sample, failing the normality (Shapiro-Wilk) test could be used as an indicator of a mixed signal (Table 3). Based upon the $\delta^{18}O$ values only, the larger size fraction at 209 kyr displays multi(bi)modality. However, the range at 209 kyr is similar to the preceding sample. In order not to spuriously reject a sample, diagnostic sedimentological features as per the study of *Scussolini et al*. [2013] were analyzed for signs of bioturbation. Based upon the coiling ratio of *G. truncatulinoides* for four successive size fractions (Figure 3a), the magnetic susceptibility (Figure 3b) and the calcium and titanium XRF counts on the bulk sediment from the core (Figures 3c and 3d), no definable signs of bioturbation are visible. For instance, should bioturbation to have affected different size fractions, as per *Bard* [2001], the abrupt transition from sinistrally dominated to dextrally dominated periods would be more gradual. Thus, our record is interpreted as being unaffected by distortions through bioturbation.

3.2. The *G. truncatulinoides*$_{dextral}$ Stable Isotopes

The single-specimen $\delta^{18}O$ signal of *G. truncatulinoides*$_{dextral}$ shows a clear distinction between the smallest and the three larger size fractions (Figure 1b) with the small specimens being, on average, ~1.5‰ more depleted in $\delta^{18}O$. This is most likely the result of a shallower calcification depth of the smaller individuals compared to the larger specimens. The latter having a longer life span precipitating larger portions of their shell at depth [*LeGrande et al*., 2004]. The range in absolute values is largest in the smallest size fraction (~2.5‰) for most samples compared to the other size fractions: 1.7‰, 1.6‰, and 1.5‰ for 250–300 μm, 300–355 μm, and 355–400 μm, respectively (Figure 4b), supporting the hypothesis that smaller-sized individuals calcify in relatively shallow water which has a larger range in temperature.

Table 3. (continued)

G. truncatulinoides (Dextral)			*G. truncatulinoides* (Sinistral)								
Combined			Covariance		Product of Standard Deviations		Correlation Coefficient		Combined		
CoVariance	Standard Deviation Product	Correlation Coefficient	212–250 μm	355–400 μm	212–250 μm	355–400 μm	212–250 μm	355–400 μm	CoVar	Standard Deviation Product	Correlation Coefficient
0.28	0.33	0.84									
0.35	0.41	0.86									
0.29	0.36	0.80							0.21	0.27	0.78
0.34	0.41	0.82	0.13	0.03	0.20	0.06	0.65	0.44	0.11	0.22	0.49
0.32	0.45	0.71	0.09	0.01	0.23	0.07	0.41	0.08			
0.49	0.60	0.81									
0.31	0.37	0.83							0.17	0.23	0.74
0.56	0.63	0.88	0.13	0.08	0.20	0.12	0.66	0.61			
0.55	0.63	0.87									
0.39	0.50	0.78									
0.44	0.53	0.83									
0.37	0.45	0.82									
0.37	0.44	0.84									
0.38	0.48	0.80									
0.20	0.28	0.70									
0.54	0.68	0.79									
0.49	0.61	0.80									
0.58	0.68	0.85							0.04	0.17	0.26
0.41	0.50	0.82	0.07	0.01	0.18	0.08	0.39	0.08	0.18	0.34	0.53
0.33	0.50	0.67	0.30	0.03	0.48	0.08	0.63	0.34			
0.41	0.58	0.71							0.17	0.29	0.58
0.28	0.49	0.57	0.16	0.10	0.28	0.20	0.58	0.51			
0.47	0.60	0.78									
0.30	0.40	0.74									
0.21	0.40	0.53									
0.20	0.45	0.45									
	Average	0.76				Average	0.55	0.34		Average	0.56

[a]Note that for *G. truncatulinoides*$_{sinistral}$, only six samples and two size fractions were analyzed.

The sample at ~232 kyr shows an unusually large range (5.3‰) and standard deviation (1.3‰) (Figure 4) caused by a shift toward values more depleted in $\delta^{18}O$ of the smallest individuals (Figure 1b). This sample at the glacial-interglacial transition (Termination III) occurred when the melting of glacial ice released cold, fresh, isotopically depleted (−38‰) water [*Broecker and Denton*, 1989], leading to a freshening and depletion in $\delta^{18}O$ of the surface water layer at the initial phase of deglaciation. While *Worthington* [1968] was the first to propose a freshwater lens over the world's oceans as a result of deglaciation, later confirmation was brought

Table 4. Shapiro-Wilk Test for Normality *p* Values for Smallest (212–250 μm) and Largest (355–400 μm) Size Fraction (for Samples Depicted in Figures 6c–6f) of Both Coiling Directions for $\delta^{18}O$ and $\delta^{13}C$[a]

	Dextral				Sinistral			
	212–250 μm		355–400 μm		212–250 μm		355–400 μm	
Age (kyr)	$\delta^{13}C$	$\delta^{18}O$	$\delta^{13}C$	$\delta^{18}O$	$\delta^{13}C$	$\delta^{18}O$	$\delta^{13}C$	$\delta^{18}O$
209	0.93	0.51	0.33	0.02[b]	0.26	0.47	0.58	0.95
211	0.31	0.25	0.04[c]	0.44	0.97	0.24	0.62	0.70
216	0.55	1.00	0.51	0.63	0.29	0.44	0.05	0.13
241	1.00	0.64	0.55	0.97	0.74	0.40	0.04[d]	0.10
243	0.64	0.53	0.16	0.94	0.16	0.14	0.61	0.81
247	0.36	0.87	0.41	0.26	0.98	0.13	0.70	0.43

[a]Samples significantly deviating from normality (b–d) show Ashman's *D* values of 6.30, 2.96, and 4.16, respectively, indicative of multi(bi)modality.

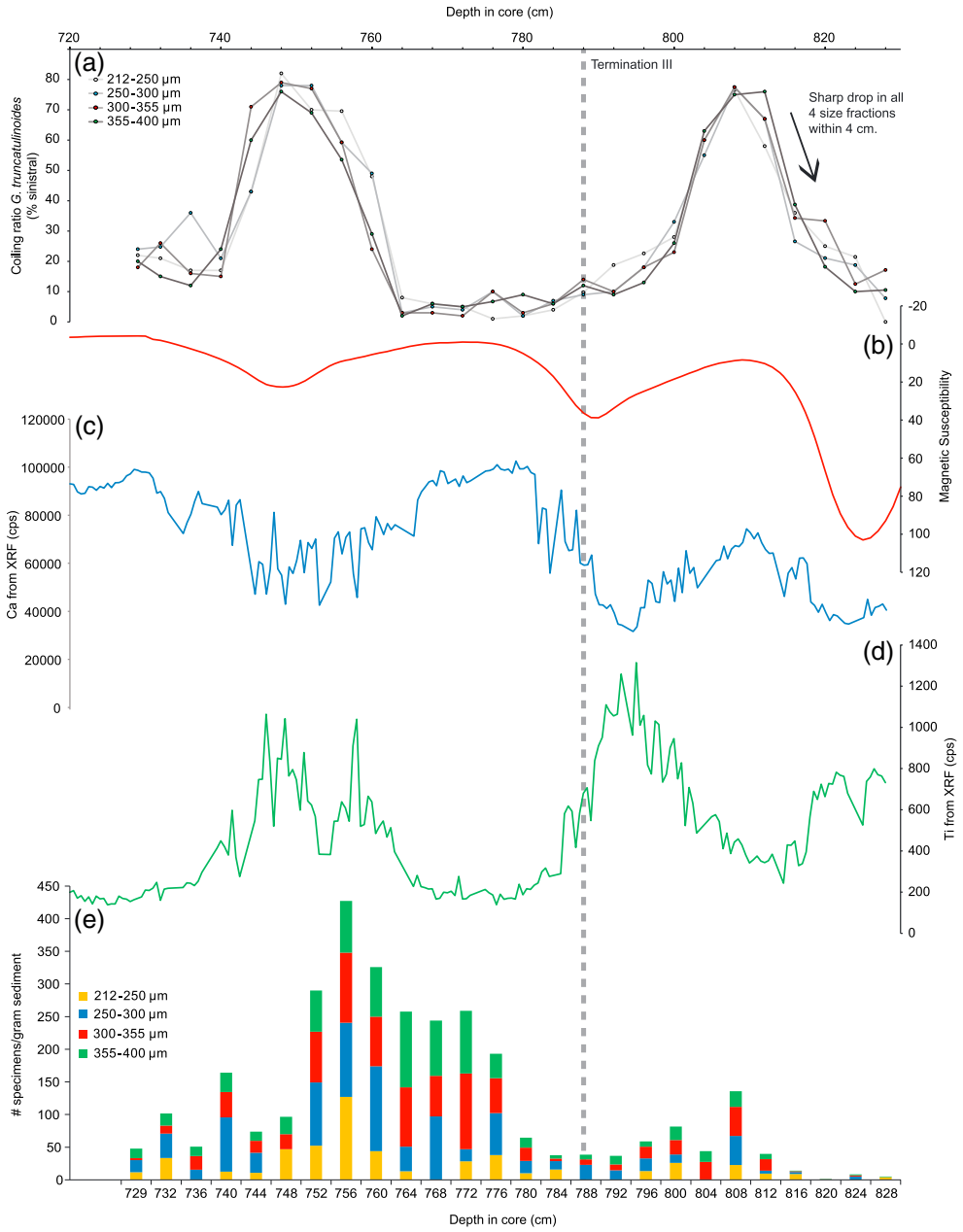

Figure 3. (a) Coiling ratio of *G. truncatulinoides* for 212–250 µm (white), 250–300 µm (blue), 300–355 µm (red), and 355–400 µm (green); (b) magnetic susceptibility at 1 cm resolution; (c) calcium and titanium; (d) elemental abundance in counts per second; and (e) abundance of *G. truncatulinoides* in number/gram sediment. The vertical dashed line is the depth of Termination III.

by *Berger* [1978] and *Berger et al.* [1977] through the unmixing of isotopic curves. *Jones and Ruddiman* [1982] considered that the melting of large-scale continental ice would have a direct effect in the local vicinity rather than an immediate global effect. Despite these findings being based on Termination I, it is plausible that there is little difference in the mechanism of freshwater input during Termination III, providing an explanation for the observed large range in $\delta^{18}O$. Small-sized individuals of *G. truncatulinoides*$_{dextral}$ likely calcified within this shallow low-salinity water lens in contrast to the largest three size fractions that remain unaffected at ~232 kyr (Figure 4b). This is caused by either (i) a drop in temperature of the surface waters due to ice rafting, yet an estimated temperature difference of 8°C amounts to a ~2‰ enrichment in $\delta^{18}O$ which would have the opposite effect or, most probably, (ii) the mixing of low-salinity water from icebergs with the upper ocean with an isotopic signature of approximately −38‰. Two more peaks with a larger total range are observed at

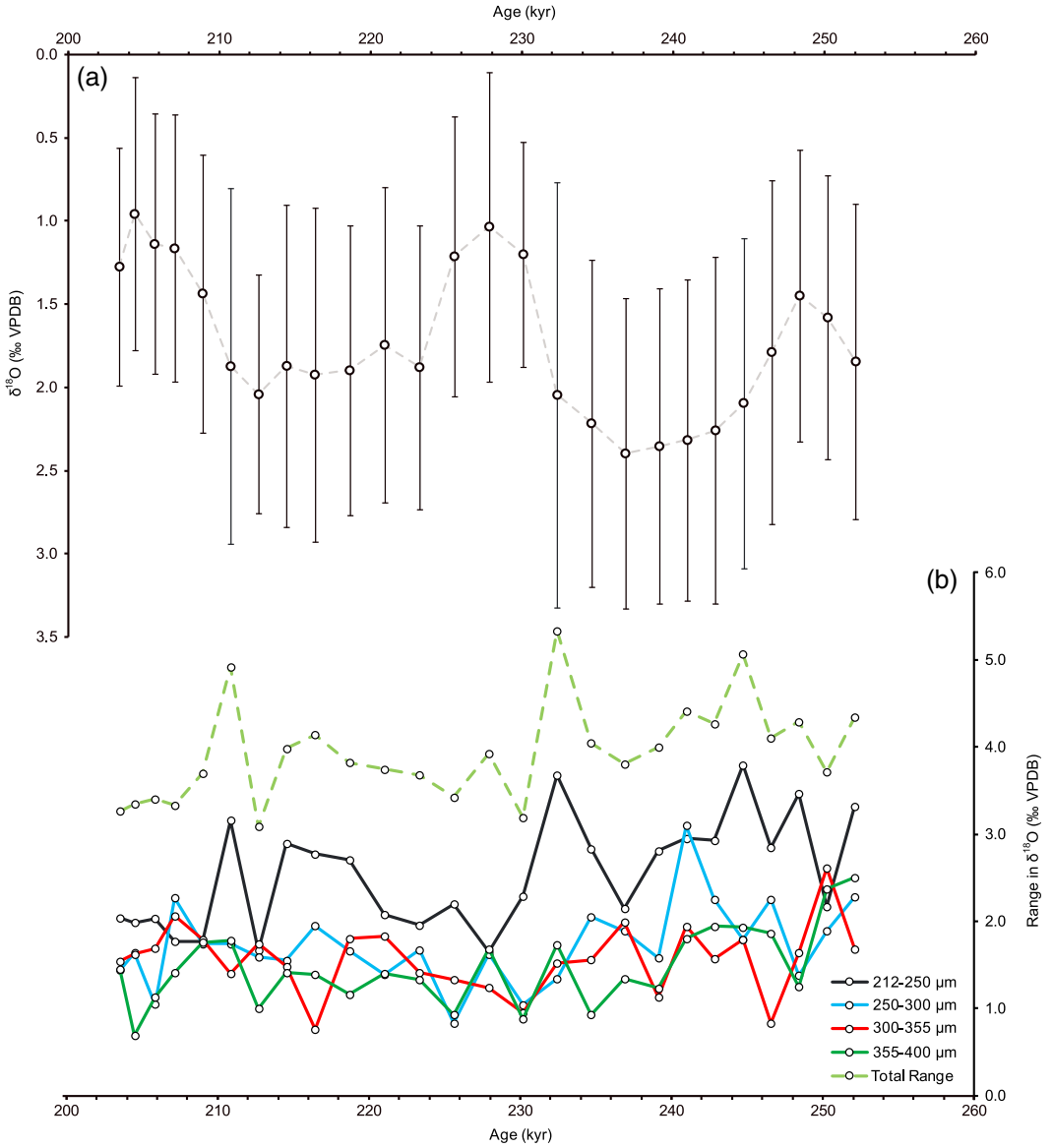

Figure 4. (a) Mean and standard deviation (error bars represent 2 standard deviations) and (b) ranges of $\delta^{18}O$ for *G. truncatulinoides*$_{dextral}$ for all four size fractions. Mean, standard deviations, and ranges are calculated by combining data for all four size fractions.

~244 kyr (5.1‰) and ~210 kyr (4.9‰) coinciding with increased numbers of particles in our core consistent with the designation ice-rafted debris (for timing correlation, see magnetic susceptibility records in *Lototskaya et al.* [1998] and *Robinson et al.* [1995]), indicating a large iceberg discharge during a HE and reflect a similar scenario of freshwater depletion in $\delta^{18}O$ values brought about by a meltwater pulse. Furthermore, there is little to no effect on the larger individuals during these HE, enabling the distinction between large- (glacial-interglacial) and small- (HE) scale climate fluctuations.

The carbon isotopes ($\delta^{13}C$) show a similar trend as the oxygen isotopes with depleted values in $\delta^{13}C$ in the smaller *G. truncatulinoides*$_{dextral}$ fraction (Figure 1c). A similar trend was observed by *Lohmann* [1995], who interprets this as secondary encrustation. He states that the $\delta^{13}C$ of the crust changes with shell size (i.e., depth of encrustment) and that all shells would have a similar $\delta^{13}C$ signal if the crust were to be removed. Furthermore, *Berger* [1978] showed, albeit for different species, a depletion in $\delta^{13}C$ with decreasing shell size.

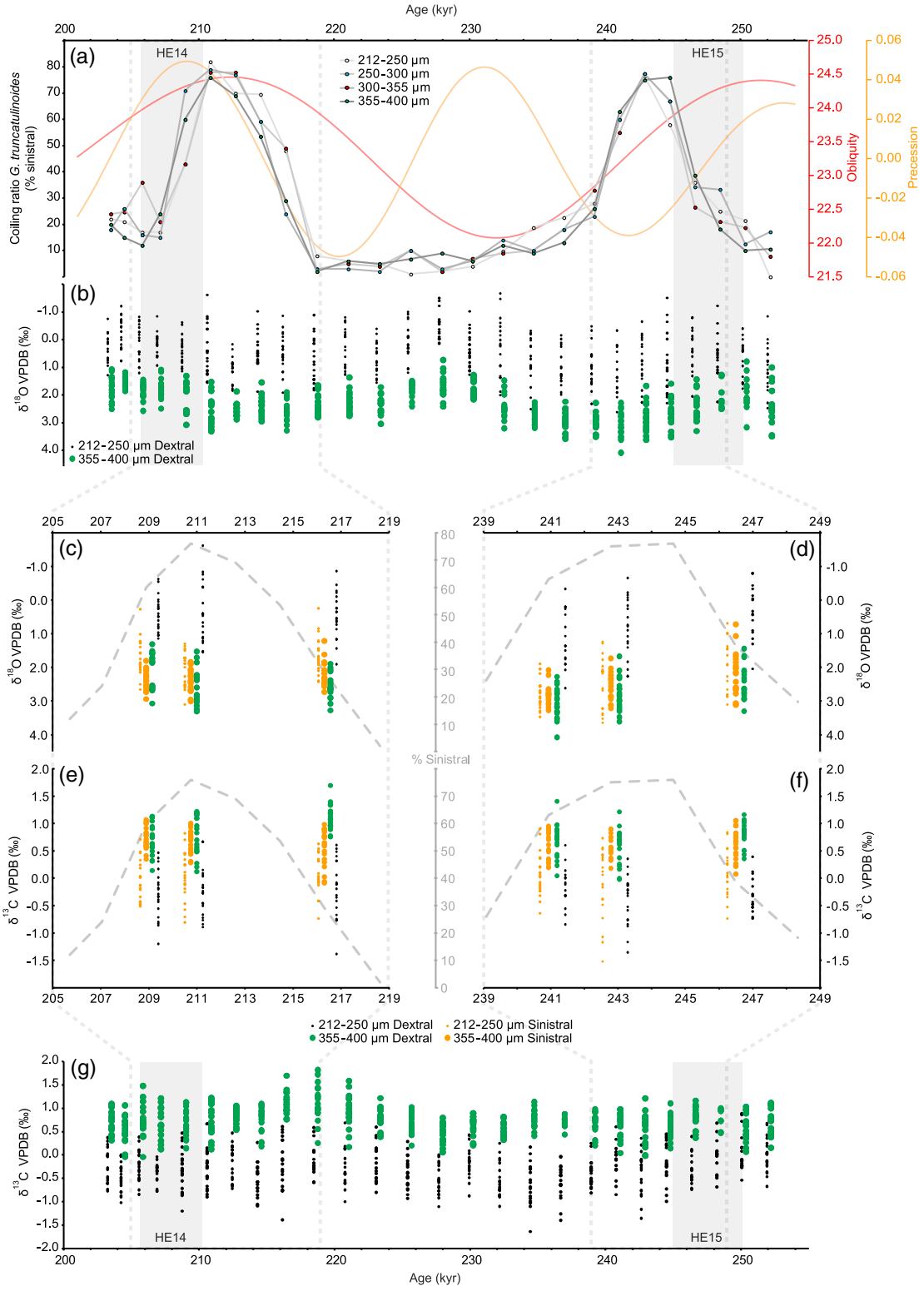

Figure 5. (a) Coiling ratio of *G. truncatulinoides* for 212–250 µm (white), 250–300 µm (blue), 300–355 µm (red), and 355–400 µm (green) with obliquity (red) and precession (orange) overlaid and *G. truncatulinoides*$_{dextral}$ single-specimen (b) $\delta^{18}O$ and (g) $\delta^{13}C$ data for 212–250 µm (black) and 355–400 µm (green). (c and e) Interglacial and (d and f) glacial comparison of single-specimen $\delta^{18}O$ (Figures 5c and 5d) and $\delta^{13}C$ (Figures 5e and 5f) data for *G. truncatulinoides*$_{dextral}$ and *G. truncatulinoides*$_{sinistral}$ of two size fractions 212–250 µm (black) and 355–400 µm (green) with coiling ratio in dashed grey. Note that single-specimen data from both size fractions of the same sample have been offset on the horizontal axis for clarification reasons. Heinrich layers 14 and 15, based on IRD abundance (Feldmeijer et al., in preparation), indicated with grey bars.

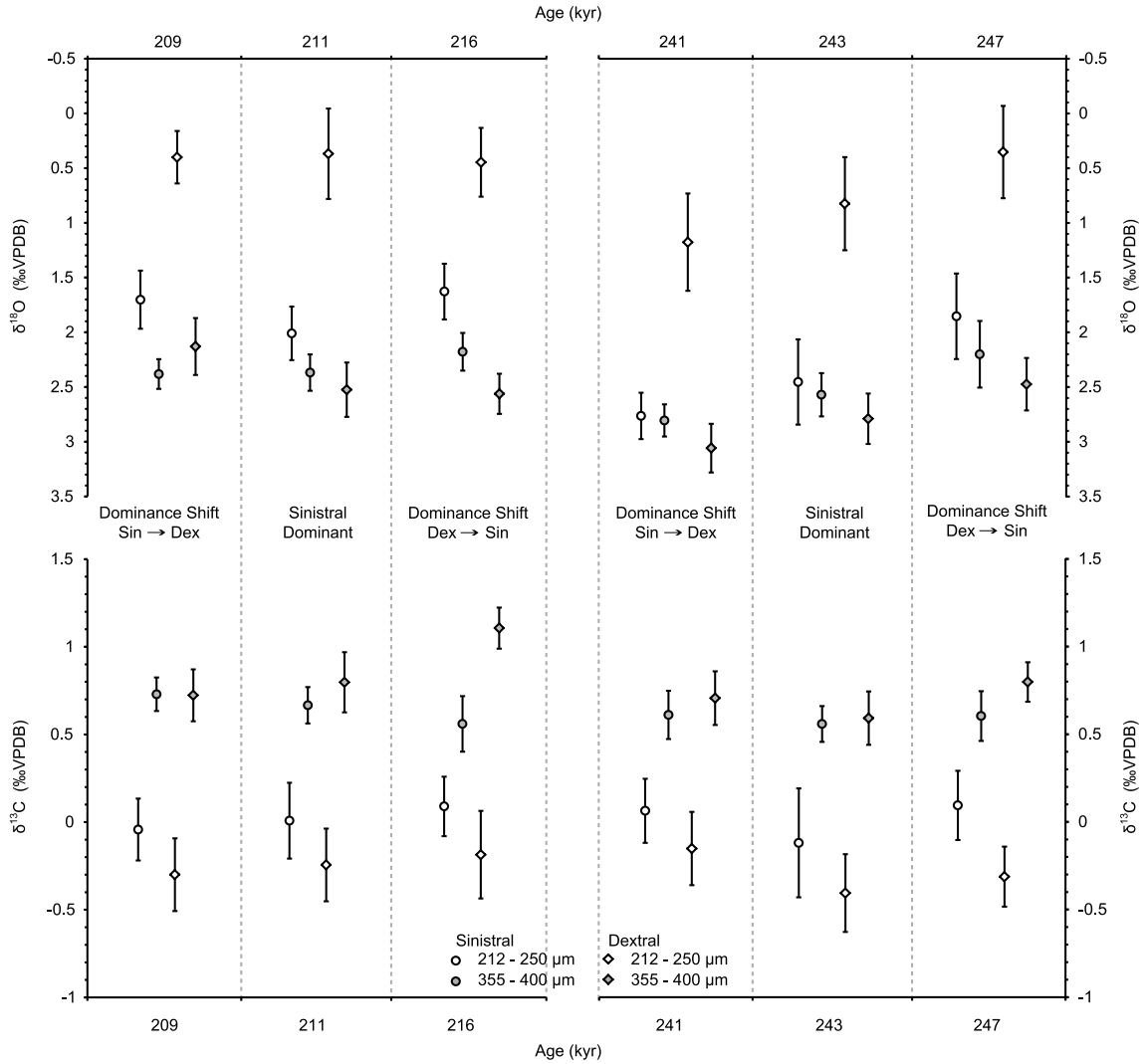

Figure 6. Comparison of the means of (top) δ^{18}O and (bottom) δ^{13}C of the smallest (open symbols) and largest (closed symbols) size fraction of both coiling directions, for the intervals defined in Figures 6c–6f. The error bars are *t*-based ($n < 30$) confidence interval on the means, based upon an $\alpha = 0.05$.

3.3. *G. truncatulinoides*$_{\text{dextral}}$ Versus *G. truncatulinoides*$_{\text{sinistral}}$

Ericson et al. [1955] mapped the regions of the North Atlantic with respect to the modern occurrence of *G. truncatulinoides*$_{\text{dextral}}$ and *G. truncatulinoides*$_{\text{sinistral}}$. Core T90-9P lies within a dextrally dominated area (up to 95% dextral), and most of our samples confirm the dominance of the right coiling variation for most of the interval studied. All four size fractions show the same trend (Figures 3a and 5a) with two peaks (~80% sinistral) in sinistral coiling specimens (~249–239 kyr and ~219–207 kyr) driven by either physical (i.e., temperature and changing movement of water bodies) or chemical (i.e., salinity or *p*H) changes in the water column [*Thiede*, 1971]. Furthermore, we found no correlation between the coiling ratio and the stable isotopes in our data set. In a modern environment, near Bermuda, the modeling study by *Lohmann and Schweitzer* [1990] infers a major decrease in *G. truncatulinoides*$_{\text{sinistral}}$ when the thermocline rises from 800 m to 600 m water depth related to the reproductive depth of sinistrally coiling specimens. This indicates that during the periods dominated by left coiling specimens, the permanent thermocline might have deepened in the water column at our core location.

The δ^{18}O results for *G. truncatulinoides*$_{\text{dextral}}$ and *G. truncatulinoides*$_{\text{sinistral}}$ for 212–250 µm and 355–400 µm (Figures 5c and 5d) strengthens the notion by *Lohmann and Schweitzer* [1990] that the sinistral coiling variety has a deeper preferred habitat or stays at greater depths for longer than the dextral coiling individuals (i.e., prefers lower temperatures). *Globorotalia truncatulinoides*$_{\text{sinistral}}$ shows statistically significant similar δ^{18}O

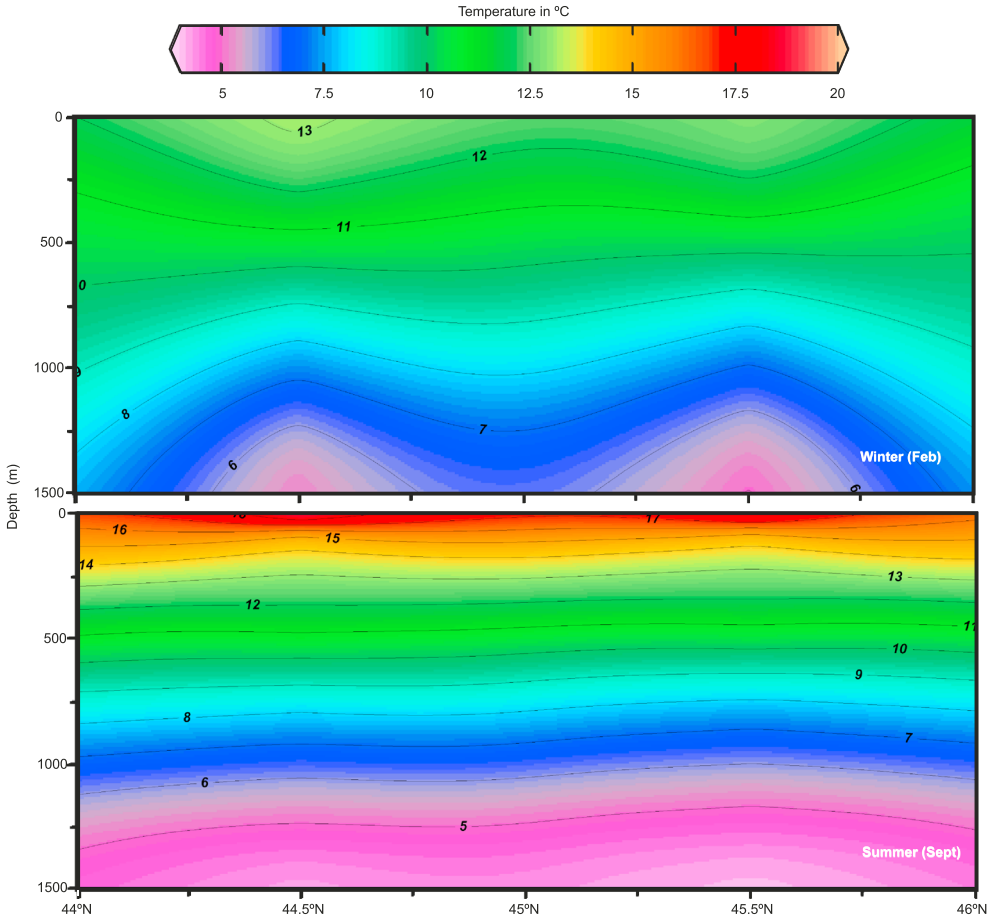

Figure 7. Temperature-depth profiles for winter and summer at core location. Data from World Ocean Atlas [*Levitus*, 2009]. Figure adapted from Ocean Data View [*Schlitzer*, 2013].

values for the two size fractions (Figure 6 and Table 2), indicating that calcification of all specimens took place within the same depth interval. The range in $\delta^{18}O$ for small and large sinistrally coiling specimens matches closely and indicates the migration of left coiling small specimens to the deeper depth habitat which was not observed with *G. truncatulinoides*$_{dextral}$. *Ujiié et al*. [2010] found, although located in the North Atlantic subtropical gyre, similar results at their most northerly station 1 from stratified plankton nets with *G. truncatulinoides*$_{sinistral}$ in 200–600 m water depth and *G. truncatulinoides*$_{dextral}$ from 100 to 200 m water depth.

A *t* test for independent samples comparing the difference between the size fraction means of a particular coiling direction concurs with the scenario of a change in the depth of the permanent thermocline (Figure 7). During the glacial, when mixing is deeper, the means are similar ($p < 0.05$; Table 3), whereas during the interglacial when the water column is more stratified, the means are different. Visually, however, the means lie close to one another (Figures 5c and 5d and Table 3), which is assumed to show that while a rise in the permanent thermocline occurs, it is weakly stratified (Figure 7). The second *t* test, that compares the difference between the means of the different coiling directions with a similar size (Table 2), shows two clear prominent features (Figure 8): (1) that the largest size fraction (355–400 μm) has, for the most part, similar carbon and oxygen isotopes that are different from the smallest size fraction and (2) the smallest size fraction has similar carbon isotopes but different oxygen isotopes.

Smaller specimens of both coiling directions are significantly more depleted in $\delta^{13}C$ than specimens >250 μm (Figures 6 and 8 and Table 3), despite a difference between the smallest size fractions in the $\delta^{18}O$ of the different coiling directions (Figure 8 and Table 2). This would indicate that the mechanism that is responsible for the difference between the oxygen isotopic composition and size (i.e., depth habitat) is different from that which alters the carbon isotopic composition. As a consequence of the surface photosynthesis and the oxidation of

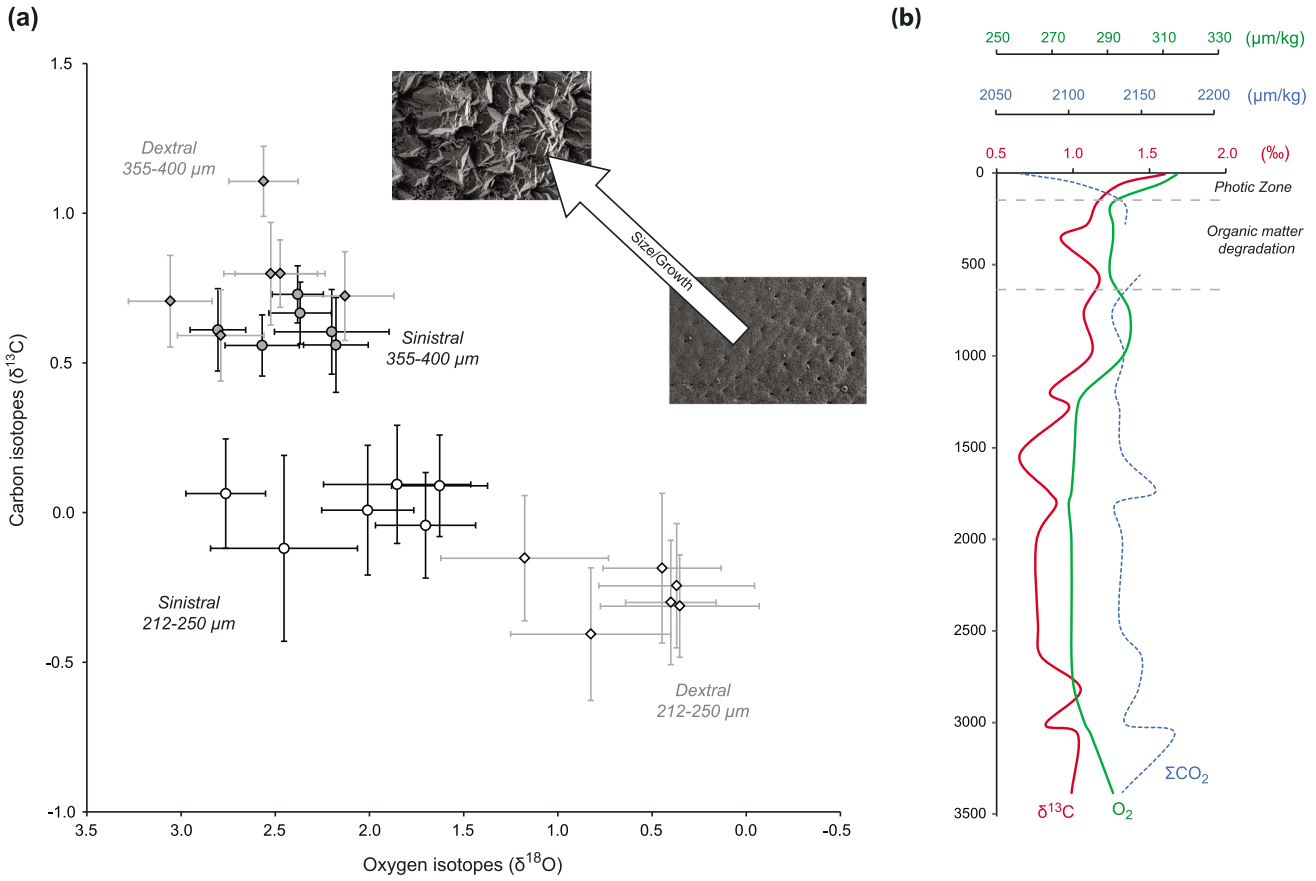

Figure 8. (a) Cross plot of average oxygen and carbon isotope values of the six samples for which both *G. truncatulinoides*$_{\text{dextral}}$ and *G. truncatulinoides*$_{\text{sinistral}}$ were analyzed (Figure 5), with *t*-based confidence intervals ($\alpha = 0.05$), showing an enrichment of oxygen isotope values and a depletion in carbon with size. This depletion is contrary to (b) the idealized carbon isotope-depth profile, based upon Station 5 (56°N) of *Kroopnick* [1980], showing total dissolved inorganic carbon (ΣCO_2), dissolved oxygen, and the carbon isotopic composition ($\delta^{13}C$) of total CO_2 which show a depletion with water depth. Although these parameters vary with depth as a consequence of surface photosynthesis, which favors ^{12}C, surface waters are enriched in $\delta^{13}C$. As the isotopically depleted organic matter sinks, it oxidizes lowering both $\delta^{13}C$ and dissolved oxygen content.

organic matter at depth the isotopic composition of dissolved inorganic carbon $\equiv \Sigma CO_2$ varies vertically, the resulting $\delta^{13}C$ profile shows enriched surface waters and prominent depleted values concordant with minima in dissolved oxygen (Figure 8). The fact that *G. truncatulinoides* is asymbiotic precludes some of the size-$\delta^{13}C$-related variance described in the literature [*Spero and DeNiro*, 1987], leaving either a dietary response [*DeNiro and Epstein*, 1978] or indicating metabolic fractionation (i.e., respiration [*Berger et al.*, 1978]) or influence on the ambient and/or internal carbon pool (i.e., carbonate ion concentration). Through feeding experiments, *Anderson et al.* [1979] showed that rather than being microherbivorous [*Lipps and Valentine*, 1970], *G. truncatulinoides* are omnivorous, feeding on both the coccolithophore *Emiliani huxleyi* and on the brine shrimp *Artemia nauplii*. In the natural environment, its abundance has been hypothesized in tracking prey concentrations, although given the considerable depths it inhabits, it likely feeds on detritus settling from the photic zone capturing prey items within its extensive, up to 8 mm surrounding the shell, rhizopodial network [*Bé et al.*, 1979]. *DeNiro and Epstein* [1978] highlighted the fact that consumers are slightly enriched in $\delta^{13}C$ from the composition of their food with each trophic level raising the $\delta^{13}C$ a process termed cumulative fraction by *McConnaughey and McRoy* [1979a, 1979b]. As photosynthesis preferentially favors ^{12}C, the organic matter produced through this pathway has typical $\delta^{13}C$ values of between -20 and -25‰; grazers are thus likely to have more depleted $\delta^{13}C$ values than carnivorous foraminifera. *Hemleben and Bijma* [1994] hypothesized that dietary change between juveniles grazing on phytoplankton, or feeding on their detritus, and the carnivorous diet of later neanic and/or adult stages should coincide with an increase in $\delta^{13}C$. Considering their depth range, and potential longevity, it would be plausible that they would undergo a change in diet or at least

the type of food available to them. Likewise, growth rate, final size, $\delta^{13}C$, and rate of chamber addition have all been shown to correlate positively with increased feeding rate [*Bé et al*., 1981; *Bijma et al*., 1992; *Hemleben et al*., 1987; *Ortiz et al*., 1996], i.e., a doubling in feeding rate resulted in a decrease in $\delta^{13}C$ by 1‰ for specimens of *Globigerinella siphonifera* [*Hemleben and Bijma*, 1994]. As metabolic rates slow, or if a reduction in food with depth occurs during ontogeny, the test becomes more enriched in ^{13}C as the incorporation of light carbon decreases [*Bemis et al*., 2000; *Berger et al*., 1978; *Birch et al*., 2013; *Fairbanks et al*., 1982; *Oppo and Fairbanks*, 1989; *Spero and Lea*, 1996; *Vincent and Berger*, 1981]. Younger (or smaller) foraminifera are inferred to have higher respiration rates (high metabolic rate thus increased kinetic fractionation), which during calcification lead to a greater amount of metabolic CO_2 depleted in ^{13}C incorporated into the test calcite [*Bemis et al*., 2000; *Berger et al*., 1978; *Ravelo and Fairbanks*, 1995].

Lohmann [1995] postulated however that the amount of secondary encrustment, with a lower $\delta^{13}C$ signal, is related to both size and water depth. The addition of a secondary crust, or gametogenetic calcite at depth, potentially via absorption and remineralization of earlier chambers and spines during preparations for reproduction, may lead to an isotopic offset [*Hemleben et al*., 1989; *Schiebel and Hemleben*, 2005]. Formation of a secondary calcite crust is in response to the temperature of the ambient environment falling below 8°C, either through seasonal fluctuations in temperature or by depth migration, which was first shown in culture by *Hemleben and Spindler* [1983] and later confirmed by downcore work [*Mulitza et al*., 1997] and sediment traps [*Spear et al*., 2011].

3.4. Paleoceanographic Implications

Therefore, assuming that the crust develops below 8°C, which at this core location varies between ~700 m and ~1000 m water depth during winter and summer, respectively (Figure 7), then this (Figures 5e and 5f) suggests that individuals >250 μm have most of the secondary crust added at or below these depths. The range in $\delta^{18}O$ corresponding to a temperature range of 8–12°C implies that *G. truncatulinoides*$_{dextral}$ <250 μm (Figure 4b) calcifies in the upper 600 m of the water column at the core location. On the other hand, *G. truncatulinoides*$_{sinistral}$ <250 μm precipitated most of its shell below this depth and based on the $\delta^{13}C$ signal not deeper than ~900 m. Furthermore, given the seasonal flux of *G. truncatulinoides* in the North Atlantic [*Storz et al*., 2009], it is safe to assume that variations among size fractions and coiling varieties are dominated by calcification depth. *Lohmann and Schweitzer* [1990] considered that *G. truncatulinoides*$_{dextral}$ sinks slower in the water column, and thus, the shallower depth habitat is a reproductive strategy to enable juvenile foraminifera, regardless of their potential migratory abilities or buoyancy control, to return to the surface with vertical mixing [*Lohmann*, 1992]. While it is evident that dextral populations increase toward the tropics and *G. truncatulinoides* in general has highest abundance in subtropical surface sediments [*Niebler*, 1995; *Pflaumann et al*., 1996] wherein mixing of the water column is restricted to the shallowest depths [*Bé*, 1977; *Ujiié et al*., 2010], other theories exist. *Healy-Williams et al*. [1985] considered that regardless of morphotype, the maximum depth habitat of *G. truncatulinoides* in the Indian Ocean had some relation to the depth of the 26.6 σ_t isopycnal; based upon Figure 3 of *Ujiié et al*. [2010], this would appear to be the case in the North Atlantic for both a well-mixed and stratified water column. If the right coiling dominance is persistently found in association with a stratified water mass [*Lohmann and Schweitzer*, 1990; *Ottens*, 1992; *Ujiié et al*., 2010], then this could indicate some association with the structure and stability of the water column that determines the dominant coiling direction. *Takayanagi et al*. [1968] identified a distinct latitudinal development of umbilical teeth on the last 2–3 chambers of the final whorl, which while independent of the coiling direction, low latitudes appear to have higher concentrations of tooth-bearing specimens. While the function of test ornamentation is not well known, umbilical teeth in the benthic foraminifer *Haynesina germanica* were identified as having some role in feeding upon diatoms [*Khanna et al*., 2013]. Living zooplankton is difficult for nonspinose foraminifera to capture and hold [*Hemleben et al*., 1985]; thus, it is likely that their diet is consistent with that of a detritivore, fluctuating with seasonal succession. In response to local hydrography from a mixed to stratified water column, the seasonal succession of the phytoplankton community changes in the North Atlantic Ocean from diatoms → flagellates, at this location presumably prymnesiophytes [*Sieracki et al*., 1993] → coccolithophores → cyanobacteria [*Veldhuis et al*., 1993]. Following deep convection in late winter, the upper ocean is supplied on average with approximately 8 μmol/L of nitrate and 6 μmol/L of silicate. The development of the seasonal thermocline during spring, in combination with this initial high initial nutrient content, favors the development of rapid-growing diatoms [*Broerse et al*., 2000], as silica is

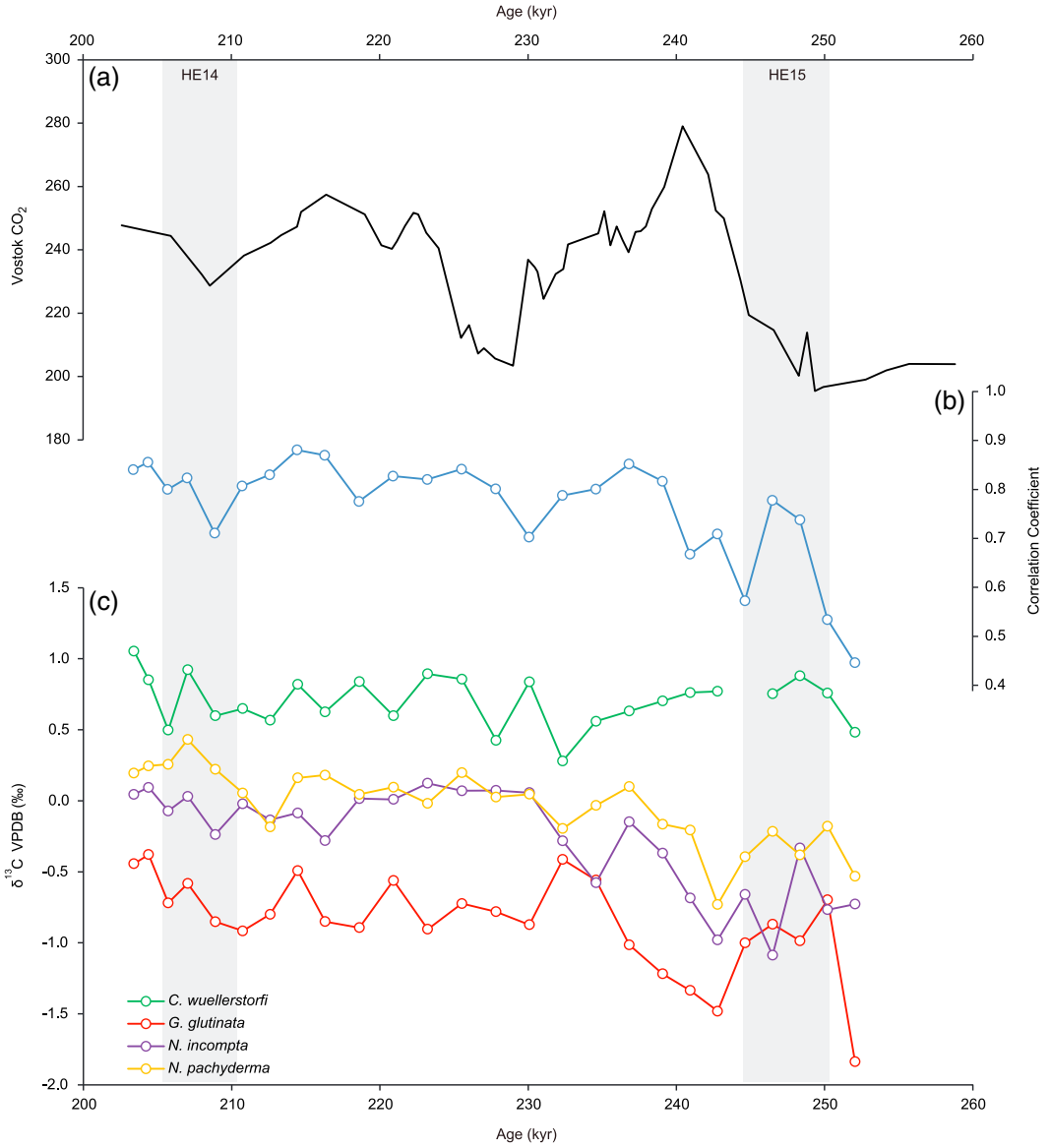

Figure 9. (a) Vostok ice core CO_2 curve from *Ruddiman and Raymo* [2003]; (b) correlation coefficient of all size fractions for *G. truncatulinoides*$_{dextral}$ (Table 3); and (c) $\delta^{13}C$ curves for the planktonic species *Globigerinita glutinata*, *Neogloboquadrina incompta*, and *Neogloboquadrina pachyderma*, and the benthic species *Cibicidoides wuellerstorfi*. Heinrich layers 14 and 15, based on IRD abundance (Feldmeijer et al., in preparation), indicated with grey bars.

depleted and the development of a stratified water column occurs; the community switches to coccolithophores suited to such oligotrophic conditions. Thus, coiling direction could have some relationship with diet, although this is purely speculation given the limited number of papers on the subject.

Certainly, the covariance between $\delta^{13}C$ and $\delta^{18}O$ of *G. truncatulinoides*$_{dextral}$ in interglacial samples would indicate some relationship between the controls of both isotopes. Intriguingly during MIS 8, this covariance is reduced. In the first instance, it could be considered that this is the combination of both the carbonate ion effect and the difference between the ice volume effect and the reorganization of carbon sinks and sources. However, when the atmospheric CO_2 concentration (Figure 9a) is compared to the covariance in $\delta^{13}C$ and $\delta^{18}O$ in *G. truncatulinoides*$_{dextral}$ and the $\delta^{13}C$ of three planktonic species *Globigerinita glutinata*, *Neogloboquadrina incompta*, and *Neogloboquadrina pachyderma*, and the benthic species *Cibicidoides wuellerstorfi*, this would appear to be incorrect. From these records, it becomes apparent that paleoceanographic shifts, apart from the ice volume effect, that have taken place over Termination III have not affected bottom waters as the $\delta^{13}C$ record of

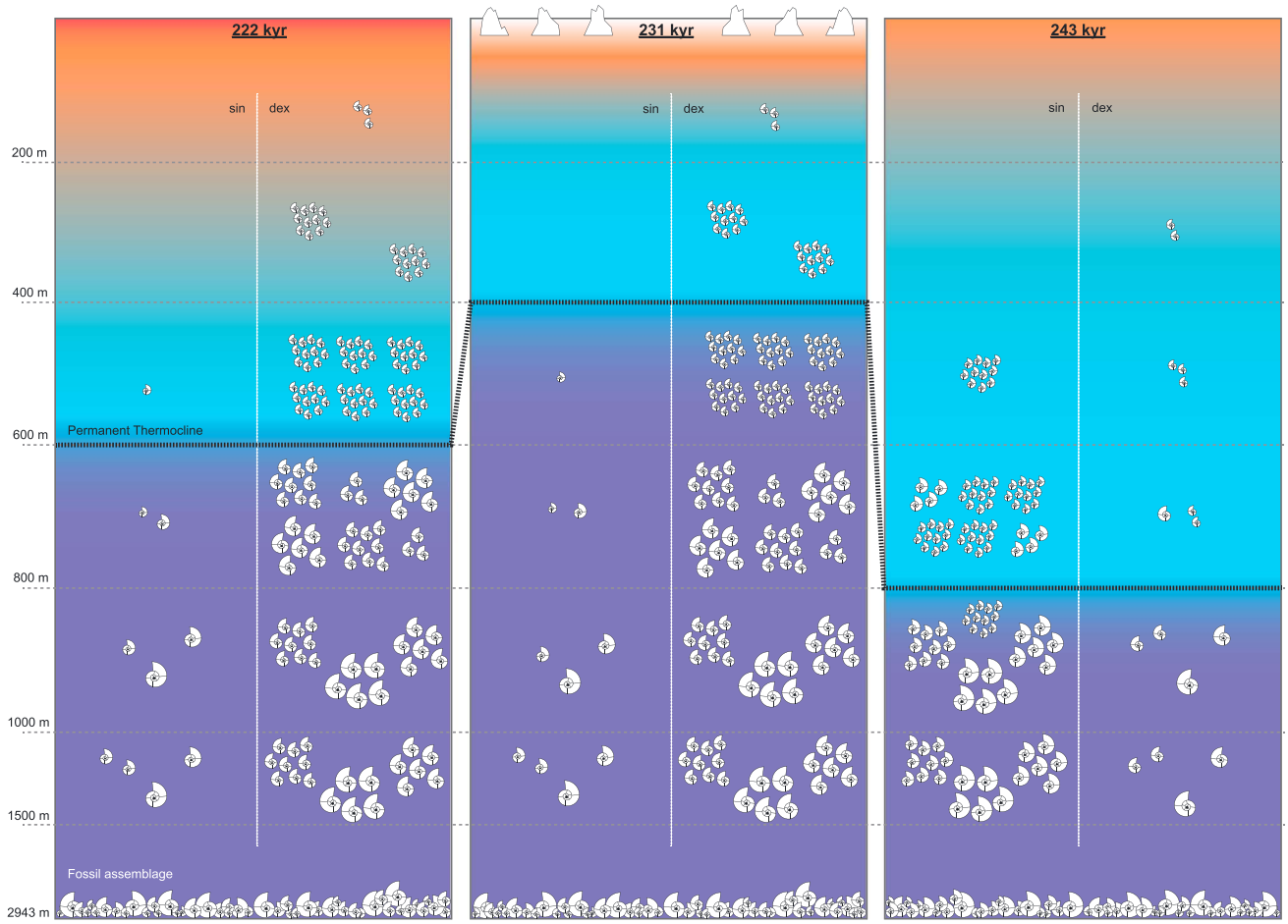

Figure 10. Schematic representation of different scenarios at 222, 231, and 243 kyr at the core location with population of *G. truncatulinoides*$_{\text{sinistral}}$ on the left side of each column and *G. truncatulinoides*$_{\text{dextral}}$ at the right. The different sizes of *G. truncatulinoides* indicate the size fractions used in this study. The color represents a relative temperature scale. Note that vertical axis (water depth) is not linear. The 243 kyr: relatively few *G. truncatulinoides*$_{\text{dextral}}$ found caused by a deepening of the permanent thermocline during the glacial period (MIS 8). Furthermore, few specimens of both coiling varieties are found in the surface waters as *G. truncatulinoides*$_{\text{sinistral}}$ prefers a deeper habitat and *G. truncatulinoides*$_{\text{dextral}}$ is nearly absent. The 231 kyr: relatively large amounts of *G. truncatulinoides*$_{\text{dextral}}$ caused by a shoaling of the permanent thermocline. Ice bergs released during the glacial-interglacial termination will cool and deplete the surface waters in δ^{18}O causing a large range in oxygen isotopes in the smallest size fraction of *G. truncatulinoides*$_{\text{dextral}}$ (Figure 3). The 222 kyr: A subsequent deepening of the permanent thermocline during the interglacial period (MIS 7) favoring *G. truncatulinoides*$_{\text{dextral}}$.

C. wuellerstorfi is remarkably stable (Figure 9c). The covariance in *G. truncatulinoides*$_{\text{dextral}}$ (Figure 9b) and the δ^{13}C record of other planktonic species (Figure 9c), however, shows very erratic behavior during the glacial period. A potential cause of these fluctuations could be the first occurrence of the coccolithophore *Emiliania huxleyi* [*Thierstein et al.*, 1977], considered to be the biggest producer of planktonic calcium carbonate [*Westbroek et al.*, 1989], instigating a large shift in the ecology of planktonic organisms and inducing a change in the carbon sinks.

From the above, a "*G. truncatulinoides* stratification index" can be reconstructed where specimens $<$250 μm of *G. truncatulinoides*$_{\text{dextral}}$ calcify in the upper 600 m of the water column and their sinistral counterparts precipitate most of their shell between 600 m and 900 m. Specimens from both coiling varieties $>$250 μm will add on chambers and secondary crust down to depths of 1000 m and potentially even deeper. This is schematically represented in Figure 10 for three snapshots in time at the core location: (i) 243 kyr during glacial times (MIS 8) dominated by *G. truncatulinoides*$_{\text{sinistral}}$ and thus the permanent thermocline at or deeper than 800 m; (ii) 231 kyr at the glacial-interglacial termination dominated by *G. truncatulinoides*$_{\text{dextral}}$ indicative of a shoaling of the permanent thermocline and, furthermore, influx of freshwater by melting glacial ice severely depleted in δ^{18}O leading to an exceptionally large range in δ^{18}O of *G. truncatulinoides*$_{\text{dextral}}$ $<$250 μm; and (iii) 222 kyr during the interglacial (MIS 7) also dominated by *G. truncatulinoides*$_{\text{dextral}}$ and the

permanent thermocline at or above 600 m water depth. The cause of the shoaling and deepening of the permanent thermocline potentially lies within the circulation of the ocean; alteration in the Atlantic meridional overturning circulation (AMOC) has been estimated to have a global impact via the propagation of Rossby/Kelvin waves [*Johnson and Marshall*, 2002]. Differential solar heating between high and low latitudes drives surface waters poleward; being disrupted by evaporation at low latitudes and the input of freshwater at high latitudes, the return of this water equatorward occurs via the sinking and formation of North Atlantic deep water in the Nordic Seas completes the AMOC component. Numerical modeling suggests that only small freshwater perturbations are sufficient to trigger significant decreases and ultimately a complete shutdown of convection. Our results indicate that the permanent thermocline responded very differently preceding Heinrich events 15 and 14, during MISs 8 and 7, respectively, potentially the result of two different forcing mechanisms. During the glacial, it is likely that the shift of deepwater convection from the Norwegian-Greenland Seas into the northern North Atlantic [*Clark et al*., 2002] means that, as per high latitudes in the modern ocean, the permanent thermocline is shallowest, to nonexistent close to or at the core location. If HE15 is in response to ice sheet instabilities instead of an oceanic forcing, then the permanent thermocline should deepen following HE15 as per our results, likely in response to a weakening of deepwater convection via input of freshwater from the HE. A conceptual model, using free ice sheet oscillations as a function of both geothermal and atmospheric processes, predicted that the Heinrich ice-rafted debris (IRD) events were accompanied by a freshwater flux to the North Atlantic on the order of only 0.16 sverdrup for 250–500 years [*MacAyeal*, 1993; *Zahn et al*., 1997]. The distribution of meltwater predominately between 40°N and 70°N disrupts and/or inhibits deepwater formation through latent melting heat, reducing oceanic heat loss, and freshwater flux that facilitates sea ice formation. The disruption of deep ocean convection reinforces itself through positive feedback through a reduction in the northward transport that prevents the salinity anomaly from being replaced by higher-salinity surface waters for an enhanced period of time [*Wiersma and Jongma*, 2010]. In contrast, HE14 appears to respond to an oceanic forcing; the deepening of the permanent thermocline appears to correspond with a rise in precession (Figure 5a). Proxy records have shown that the AMOC was at its weakest in the preceding 1–2 kyr from the onset of certain Heinrich events; the subsurface heating associated with this AMOC reduction through the downward mixing of heat that continued at low latitudes significantly increased the rate of mass loss of ice sheets initiating the HE [*Bond and Lotti*, 1995; *Gutjahr et al*., 2010; *Mangini et al*., 2010; *Marcott et al*., 2011; *McManus et al*., 2004; *Zahn et al*., 1997]. The shoaling of the permanent thermocline, initiated by the HE-induced meltwater event, leads into the return of glacial-like conditions that mark MIS 7.

4. Conclusion and Outlook

This study shows the importance of analyzing single specimens from multiple size fractions of both *G. truncatulinoides*$_{dextral}$ and *G. truncatulinoides*$_{sinistral}$ as it provides a good indication for the relative depth of the permanent (paleo)thermocline. Especially in sample locations where both coiling varieties and shifts in dominance between one and the other coiling direction are found over time, one can make a relative estimate of the depth at which the permanent thermocline must have been. Furthermore, this *G. truncatulinoides* stratification index quantifies large-scale ocean changes in terms of vertical stratification. Applied in highly resolved time slices over a latitudinal gradient, it will give an indication of rates and magnitudes of climate perturbations.

Acknowledgments
The manuscript has benefitted greatly from comments of P. deMenocal and five anonymous reviewers. Core scanning was supported by the Netherlands Organization for Scientific Research (NWO) through the SCAN2 program on advanced instrumentation. This is a contribution to the Darwin Center for Biogeosciences project "Sensing Seasonality" and the NWO open round funded "Digging for density." For data supporting this article, please contact W. Feldmeijer (w.feldmeijer@vu.nl) or B. Metcalfe (b.metcalfe@vu.nl).

References

Anderson, O. R., M. Spindler, A. W. H. Be, and C. Hemleben (1979), Trophic activity of planktonic foraminifera, *J. Mar. Biol. Assoc. U. K.*, *59*, 791–799.

Ashman, K. M., C. M. Bird, and S. E. Zepf (1994), Detecting bimodality in astronomical datasets, *Astron. J.*, *108*(6), 2348–2361.

Bard, E. (2001), Paleoceanographic implications of the difference in deep-sea sediment mixing between large and fine particles, *Paleoceanography*, *16*(3), 235–239, doi:10.1029/2000PA000537.

Bé, A. W. H. (1960), Ecology of recent planktonic foraminifera: Part 2—Bathymetric and seasonal distributions in the Sargasso Sea off Bermuda, *Micropaleontology*, *6*(4), 373–392.

Bé, A. W. H. (1977), An ecological, zoogeographic, and taxonomic review of recent planktonic foraminifera, in *Oceanic Micropalaeontology*, edited by A. T. S. Ramsay, pp. 1–100, Academic Press, London.

Bé, A. W. H., C. Hemleben, O. R. Anderson, and M. Spindler (1979), Chamber formation in planktonic foraminifera, *Micropaleontology*, *25*, 294–307.

Bé, A. W. H., D. A. Caron, and O. R. Anderson (1981), Effects of feeding frequency on life processes of the planktonic foraminifer *Globigerinoides sacculifer* in laboratory culture, *J. Mar. Biol. Assoc. U. K.*, *61*, 257–277.

Bé, A. W. H., J. K. B. Bishop, M. S. Sverdlove, and W. D. Gardner (1985), Standing stock, vertical distribution and flux of planktonic foraminifera in the Panama Basin, *Mar. Micropaleontol.*, *9*(4), 307–333.
Bemis, B. E., H. J. Spero, D. W. Lea, and J. Bijma (2000), Temperature influence on the carbon isotopic composition of *Globigerina bulloides* and *Orbulina universa* (planktonic foraminifera), *Mar. Micropaleontol.*, *38*(3), 213–228.
Berger, W. H. (1978), Oxygen-18 stratigraphy in deep-sea sediments: Additional evidence for the deglacial meltwater effect, *Deep Sea Res.*, *25*(5), 473–479.
Berger, W. H., R. F. Johnson, and J. S. Killingley (1977), "Unmixing" of the deep-sea record and the deglacial meltwater spike, *Nature*, *269*(5630), 661–663.
Berger, W. H., J. Killingley, and E. Vincent (1978), Sable isotopes in deep-sea carbonates-box core ERDC-92, west equatorial Pacific, *Oceanol. Acta*, *1*(2), 203–216.
Bijma, J., C. Hemleben, H. Oberhaensli, and M. Spindler (1992), The effects of increased water fertility on tropical spinose planktonic foraminifers in laboratory cultures, *J. Foraminiferal Res.*, *22*(3), 242–256.
Birch, H., H. K. Coxall, P. N. Pearson, D. Kroon, and M. O'Regan (2013), Planktonic foraminifera stable isotopes and water column structure: Disentangling ecological signals, *Mar. Micropaleontol.*, *101*, 127–145.
Bolli, H. (1950), The direction of coiling in the evolution of some Globorotaliidae, *Contrib. Cushman Found. Foraminiferal Res.*, *1*, 82–89.
Bolli, H. (1951), Notes on the direction of coiling of rotalid foraminifera, *Contr. Cushman Found. Foram. Res.*, *2*, 139–143.
Bond, G. C., and R. Lotti (1995), Iceberg discharges into the North Atlantic on millenial time scales during the last glaciation, *Science*, *267*, 1005–1010.
Broecker, W. S., and G. H. Denton (1989), The role of ocean-atmosphere reorganizations in glacial cycles, *Geochim. Cosmochim. Acta*, *53*(10), 2465–2501.
Broerse, A. T. C., P. Ziveri, J. E. van Hinte, and S. Honjo (2000), Coccolithophore export production, species composition, and coccolith-CaCO3 fluxes in the NE Atlantic (34°N, 21°W and 48°N, 21°W), *Deep Sea Res., Part II*, *47*(9), 1877–1905.
Brummer, G., and D. Kroon (1988), Genetically controlled planktonic foraminiferal coiling ratios as tracers of past ocean dynamics, in *Planktonic Foraminifers as Tracers of Ocean-Climate History*, pp. 293–298, Free Univ. Press, Amsterdam.
Cheng, H., R. L. Edwards, W. S. Broecker, G. H. Denton, X. Kong, Y. Wang, R. Zhang, and X. Wang (2009), Ice age terminations, *Science*, *326*(5950), 248–252.
Clark, P. U., N. G. Pisias, T. F. Stocker, and A. J. Weaver (2002), The role of the thermohaline circulation in abrupt climate change, *Nature*, *415*(6874), 863–869.
Cléroux, C., E. Cortijo, J.-C. Duplessy, and R. Zahn (2007), Deep-dwelling foraminifera as thermocline temperature recorders, *Geochem. Geophys. Geosyst.*, *8*, Q04N11, doi:10.1029/2006GC001474.
Darling, K. F., C. M. Wade, D. Kroon, and A. J. L. Brown (1997), Planktic foraminiferal molecular evolution and their polyphyletic origins from benthic taxa, *Mar. Micropaleontol.*, *30*(4), 251–266.
DeNiro, M. J., and S. Epstein (1978), Influence of diet on the distribution of carbon isotopes in animals, *Geochim. Cosmochim. Acta*, *42*(5), 495–506.
Deuser, W. G., and E. H. Ross (1989), Seasonally abundant planktonic foraminifera of the Sargasso Sea: Succession, deep-water fluxes, isotopic compositions, and paleoceanographic implications, *J. Foraminiferal Res.*, *19*(4), 268–293.
Deuser, W. G., E. H. Ross, C. Hemleben, and M. Spindler (1981), Seasonal changes in species composition, numbers, mass, size, and isotopic composition of planktonic foraminifera settling into the deep Sargasso Sea, *Palaeogeogr. Palaeoclimatol. Palaeoecol.*, *33*(1), 103–127.
de Vargas, C., S. Renaud, H. Hilbrecht, and J. Pawlowski (2001), Pleistocene adaptive radiation in *Globorotalia truncatulinoides*: Genetic, morphologic, and environmental evidence, *Paleobiology*, *27*(1), 104–125.
d'Orbigny, A. D. (1839), Foraminifères, in *Histoire Naturelle des Iles Canaries, Zoologie*, vol. 2, edited by P. Barker-Webb and S. Berthelot, pp. 119–146, Arthus Bertrand, Paris.
Dowsett, H. J. (1989), Application of the graphic correlation method to Pliocene marine sequences, *Mar. Micropaleontol.*, *14*(1), 3–32.
Durazzi, J. T. (1981), Stable-isotope studies of planktonic foraminifera in North Atlantic core tops, *Palaeogeogr. Palaeoclimatol. Palaeoecol.*, *33*(1–3), 157–172.
Eguchi, N. O., H. Kawahata, and A. Taira (1999), Seasonal response of planktonic foraminifera to surface ocean condition: Sediment trap results from the central North Pacific Ocean, *J. Oceanogr.*, *55*(6), 681–691.
Erez, J., and S. Honjo (1981), Comparison of isotopic composition of planktonic foraminifera in plankton tows, sediment traps, and sediments, *Palaeogeogr. Palaeoclimatol. Palaeoecol.*, *33*(1–3), 129–156.
Ericson, D. B., G. Wollin, and J. Wollin (1955), Coiling direction of *Globorotalia truncatulinoides* in deep-sea cores, *Deep Sea Res.*, *2*(2), 152–158.
Fairbanks, R. G., M. Sverdlove, R. Free, P. H. Wiebe, and A. W. Bé (1982), Vertical distribution and isotopic fractionation of living planktonic foraminifera from the Panama Basin, *Nature*, *298*(5877), 841–844.
Ganssen, G., F. Peeters, B. Metcalfe, P. Anand, S. Jung, D. Kroon, and G. Brummer (2011), Quantifying sea surface temperature ranges of the Arabian Sea for the past 20,000 years, *Clim. Past*, *7*, 1337–2686.
Gutjahr, M., B. A. A. Hoogakker, M. Frank, and I. N. McCave (2010), Changes in North Atlantic deep water strength and bottom water masses during marine isotope stage 3 (45–35 ka B.P.), *Quat. Sci. Rev.*, *29*(19), 2451–2461.
Hammer, Ø., D. A. T. Harper, and P. D. Ryan (2001), PAST: Paleontological statistics software package for education and data analysis, *Palaeontol. Electron.*, *4*(1), 9.
Hays, J. D., and W. Berggren (1971), Quaternary boundaries and correlations, in *The Micropaleontology of Oceans*, pp. 669–691, Cambridge Univ. Press, Cambridge, U. K.
Healy-Williams, N., and D. F. Williams (1981), Fourier analysis of test shape of planktonic foraminifera, *Nature*, *289*, 485–487.
Healy-Williams, N., R. Ehrlich, and D. F. Williams (1985), Morphometric and stable isotopic evidence for subpopulations of *Globorotalia truncatulinoides*, *J. Foraminiferal Res.*, *15*(4), 242–253.
Hemleben, C., and J. Bijma (1994), Foraminiferal population dynamics and stable carbon isotopes, in *Carbon Cycling in the Glacial Ocean: Constraints on the Ocean's Role in Global Change*, pp. 145–166, Springer, Berlin.
Hemleben, C., and M. Spindler (1983), Recent advances in research on living planktonic foraminifera, in *Reconstruction of Marine Paleoenvironments*, edited by J. E. Meulenkamp, *Utrecht Micropaleontol. Bull.*, *30*, 141–170.
Hemleben, C., M. Spindler, I. Breitinger, and W. G. Deuser (1985), Field and laboratory studies on the ontogeny and ecology of some globorotaliid species from the Sargasso Sea off Bermuda, *J. Foraminiferal Res.*, *15*(4), 254–272.
Hemleben, C., M. Spindler, I. Breitinger, and R. Ott (1987), Morphological and physiological responses of *Globigerinoides sacculifer* (Brady) under varying laboratory conditions, *Mar. Micropaleontol.*, *12*, 305–324.

Hemleben, C., M. Spindler, and O. R. Anderson (1989), *Modern Planktonic Foraminifera*, 363 pp., Springer, New York.
Huybers, P. (2007), Glacial variability over the last two million years: An extended depth-derived agemodel, continuous obliquity pacing, and the Pleistocene progression, *Quat. Sci. Rev.*, *26*(1–2), 37–55.
Johnson, H. L., and D. P. Marshall (2002), A theory for the surface Atlantic response to thermohaline variability, *J. Phys. Oceanogr.*, *32*(4), 1121–1132.
Jones, G. A., and W. F. Ruddiman (1982), Assessing the global meltwater spike, *Quat. Res.*, *17*(2), 148–172.
Kemle-von Mücke, S., and C. Hemleben (1999), Foraminifera, *S. Atl. Zooplankton*, *1*, 43–73.
Kennett, J. P. (1968), *Globorotalia truncatulinoides* as a paleo-oceanographic index, *Science*, *159*(3822), 1461–1463.
Kennett, J. P. (1970), Pleistocene paleoclimates and foraminiferal biostratigraphy in subantarctic deep-sea cores, *Deep Sea Res. Oceanogr. Abstr.*, *17*, 125–140.
Khanna, N., J. A. Godbold, W. E. N. Austin, and D. M. Paterson (2013), The impact of ocean acidification on the functional morphology of foraminifera, *PLoS One*, *8*(12), e83118.
Killingley, J. S., R. F. Johnson, and W. H. Berger (1981), Oxygen and carbon isotopes of individual shells of planktonic foraminifera from Ontong-Java plateau, equatorial Pacific, *Palaeogeogr. Palaeoclimatol. Palaeoecol.*, *33*(1–3), 193–204.
Kroopnick, P. (1980), The distribution of ^{13}C in the Atlantic Ocean, *Earth Planet. Sci. Lett.*, *49*(2), 469–484.
Lazarus, D., H. Hilbrecht, C. Spencer-Cervato, and H. Thierstein (1995), Sympatric speciation and phyletic change in *Globorotalia truncatulinoides*, *Paleobiology*, *21*, 28–51.
LeGrande, A. N., J. Lynch-Stieglitz, and E. C. Farmer (2004), Oxygen isotopic composition of *Globorotalia truncatulinoides* as a proxy for intermediate depth density, *Paleoceanography*, *19*, PA4025, doi:10.1029/2004PA001045.
Levitus, S. (2009), *WOA09*, 184 pp., U.S. Gov. Print. Off., Washington, D. C.
Lipps, J., and J. Valentine (1970), The role of foraminifera in the trophic structure of marine communities, *Lethaia*, *3*(3), 279–286.
Lohmann, G. P. (1992), Increasing seasonal upwelling in the subtropical South Atlantic over the past 700,000 years: Evidence from deep-living planktonic foraminifera, *Mar. Micropaleontol.*, *19*, 1–12.
Lohmann, G. P. (1995), A model for variation in the chemistry of planktonic foraminifera due to secondary calcification and selective dissolution, *Paleoceanography*, *10*(3), 445–457, doi:10.1029/95PA00059.
Lohmann, G. P., and B. A. Malmgren (1983), Equatorward migration of *Globorotalia truncatulinoides* ecophenotypes through the late Pleistocene: Gradual evolution or ocean change?, *Paleobiology*, *9*(4), 414–421.
Lohmann, G. P., and P. N. Schweitzer (1990), *Globorotalia truncatulinoides*' growth and chemistry as probes of the past thermocline: 1. Shell size, *Paleoceanography*, *5*(1), 55–75, doi:10.1029/PA005i001p00055.
Lončarić, N., G.-J. A. Brummer, and D. Kroon (2005), Lunar cycles and seasonal variations in deposition fluxes of planktic foraminiferal shell carbonate to the deep South Atlantic (central Walvis Ridge), *Deep Sea Res., Part I*, *52*(7), 1178–1188.
Lončarić, N., J. van Iperen, D. Kroon, and G.-J. A. Brummer (2007), Seasonal export and sediment preservation of diatomaceous, foraminiferal, and organic matter mass fluxes in a trophic gradient across the SE Atlantic, *Prog. Oceanogr.*, *73*(1), 27–59.
Lototskaya, A., P. Ziveri, G. M. Ganssen, and J. E. van Hinte (1998), Calcareous nannofloral response to Termination II at 45°N, 25°W (northeast Atlantic), *Mar. Micropaleontol.*, *34*(1–2), 47–70.
MacAyeal, D. R. (1993), Binge/purge oscillations of the Laurentide ice sheet as a cause of the North Atlantic's Heinrich events, *Paleoceanography*, *8*(6), 775–784, doi:10.1029/93PA02200.
Mangini, A., J. M. Godoy, M. L. Godoy, R. Kowsmann, G. M. Santos, M. Ruckelshausen, A. Schroeder-Ritzrau, and L. Wacker (2010), Deep sea corals off Brazil verify a poorly ventilated Southern Pacific Ocean during H2, H1, and the Younger Dryas, *Earth Planet. Sci. Lett.*, *293*(3), 269–276.
Marcott, S. A., P. U. Clark, L. Padman, G. P. Klinkhammer, S. R. Springer, Z. Liu, B. L. Otto-Bliesner, A. E. Carlson, A. Ungerer, and J. Padman (2011), Ice-shelf collapse from subsurface warming as a trigger for Heinrich events, *Proc. Natl. Acad. Sci. U.S.A.*, *108*(33), 13,415–13,419.
Martínez, J. I. (1994), Late Pleistocene palaeocenography of the Tasman Sea: Implications for the dynamics of the warm pool in the western Pacific, *Palaeogeogr. Palaeoclimatol. Palaeoecol.*, *112*(1–2), 19–62.
Martínez, J. I. (1997), Decreasing influence of Subantarctic Mode Water north of the Tasman Front over the past 150 kyr, *Palaeogeogr. Palaeoclimatol. Palaeoecol.*, *131*(3–4), 355–364.
McConnaughey, T., and C. McRoy (1979a), Food-web structure and the fractionation of carbon isotopes in the Bering Sea, *Mar. Biol.*, *53*(3), 257–262.
McConnaughey, T., and C. McRoy (1979b), ^{13}C label identifies eelgrass (Zostera marina) carbon in an Alaskan estuarine food web, *Mar. Biol.*, *53*(3), 263–269.
McManus, J. F., R. Francois, J.-M. Gherardi, L. D. Keigwin, and S. Brown-Leger (2004), Collapse and rapid resumption of Atlantic meridional circulation linked to deglacial climate changes, *Nature*, *428*(6985), 834–837.
Mulitza, S., A. Dürkoop, W. Hale, G. Wefer, and H. S. Niebler (1997), Planktonic foraminifera as recorders of past surface-water stratification, *Geology*, *25*(4), 335–338.
Niebler, H.-S. (1995), Reconstruction of paleo-environmental parameters using stable isotopes and faunal assemblages of planktonic foraminifera in the South Atlantic Ocean, Berichte zur Polarforschung (Reports on Polar Research), 167.
Oppo, D. W., and R. G. Fairbanks (1989), Carbon isotope composition of tropical surface water during the past 22,000 years, *Paleoceanography*, *4*(4), 333–351, doi:10.1029/PA004i004p00333.
Ortiz, J., A. Mix, W. Rugh, J. Watkins, and R. Collier (1996), Deep-dwelling planktonic foraminifera of the northeastern Pacific Ocean reveal environmental control of oxygen and carbon isotopic disequilibria, *Geochim. Cosmochim. Acta*, *60*(22), 4509–4523.
Ottens, J. J. (1992), Spatial dynamics of planktic foraminifera in the Northeast Atlantic, in *Planktonic Foraminifera as Indicators of Ocean Environments in the Northeast Atlantic*, thesis, pp. 109–147, Vrije Univ., Amsterdam.
Pflaumann, U., J. Duprat, C. Pujol, and L. D. Labeyrie (1996), SIMMAX: A modern analog technique to deduce Atlantic Sea surface temperatures from planktonic foraminifera in deep-sea sediments, *Paleoceanography*, *11*(1), 15–35, doi:10.1029/95PA01743.
Pharr, R. B., and D. F. Williams (1987), Shape changes in *Globorotalia truncatulinoides* as a function of ontogeny and paleobiogeography in the Southern Ocean, *Mar. Micropaleontol.*, *12*, 343–355.
Pinet, P. R. (2009), *Invitation to Oceanography*, Jones & Bartlett Publishers, Burlington.
Quillévéré, F., R. Morard, G. Escarguel, C. J. Douady, Y. Ujiié, T. de Garidel-Thoron, and C. De Vargas (2011), Global scale same-specimen morpho-genetic analysis of *Truncorotalia truncatulinoides*: A perspective on the morphological species concept in planktonic foraminifera, *Palaeogeogr. Palaeoclimatol. Palaeoecol.*, *391*, 2–12.
Ravelo, A. C., and R. G. Fairbanks (1992), Oxygen isotopic composition of multiple species of planktonic foraminifera: Recorders of the modern photic zone temperature gradient, *Paleoceanography*, *7*(6), 815–831, doi:10.1029/92PA02092.

Ravelo, A. C., and R. G. Fairbanks (1995), Carbon isotopic fractionation in multiple species of planktonic foraminifera from core tops in the tropical Atlantic, *J. Foramineferal Res.*, *25*(1), 53–74.
Renaud, S., and D. N. Schmidt (2003), Habitat tracking as a response of the planktic foraminifer *Globorotalia truncatulinoides* to environmental fluctuations during the last 140 kyr, *Mar. Micropaleontol.*, *49*(1–2), 97–122.
Robinson, S. G., M. A. Maslin, and I. N. McCave (1995), Magnetic susceptibility variations in Upper Pleistocene deep-sea sediments of the NE Atlantic: Implications for ice rafting and paleocirculation at the Last Glacial Maximum, *Paleoceanography*, *10*(2), 221–250, doi:10.1029/94PA02683.
Ruddiman, W. F. (2001), *Earth's Climate: Past and Future*, W. H. Freeman and Company, New York.
Ruddiman, W. F., and M. E. Raymo (2003), A methane-based time scale for Vostok ice, *Quat. Sci. Rev.*, *22*(2), 141–155.
Schiebel, R., and C. Hemleben (2005), Modern planktic foraminifera, *Paläont. Z.*, *79*(1), 135–148.
Schlitzer, R. (2013), Ocean Data View, edited. [Available at http://odv.awi.de.]
Scussolini, P., E. van Sebille, and J. V. Durgadoo (2013), Paleo Agulhas rings enter the subtropical gyre during the penultimate deglaciation, *Clim. Past*, *9*(6), 2631–2639.
Sexton, P. F., and R. D. Norris (2008), Dispersal and biogeography of marine plankton: Long-distance dispersal of the foraminifer *Truncorotalia truncatulinoides*, *Geology*, *36*(11), 899–902.
Sieracki, M. E., P. G. Verity, and D. K. Stoecker (1993), Plankton community response to sequential silicate and nitrate depletion during the 1989 North Atlantic spring bloom, *Deep Sea Res., Part II*, *40*(1), 213–225.
Spear, J. W., R. Z. Poore, and T. M. Quinn (2011), *Globorotalia truncatulinoides* (dextral) Mg/Ca as a proxy for Gulf of Mexico winter mixed-layer temperature: Evidence from a sediment trap in the northern Gulf of Mexico, *Mar. Micropaleontol.*, *80*(3–4), 53–61.
Spencer-Cervato, C., and H. R. Thierstein (1997), First appearance of *Globorotalia truncatulinoides*: Cladogenesis and immigration, *Mar. Micropaleontol.*, *30*(4), 267–291.
Spero, H. J., and M. DeNiro (1987), The influence of symbiont photosynthesis on the $\delta^{18}O$ and $\delta^{13}C$ values of planktonic foraminiferal shell calcite, *Symbiosis*, *4*(1–3), 213–228.
Spero, H. J., and D. W. Lea (1996), Experimental determination of stable isotope variability in *Globigerina bulloides*: Implications for paleoceanographic reconstructions, *Mar. Micropaleontol.*, *28*, 231–246.
Steph, S., M. Regenberg, R. Tiedemann, S. Mulitza, and D. Nürnberg (2009), Stable isotopes of planktonic foraminifera from tropical Atlantic/Caribbean core tops: Implications for reconstructing upper ocean stratification, *Mar. Micropaleontol.*, *71*(1–2), 1–19.
Storz, D., H. Schulz, J. J. Waniek, D. E. Schulz-Bull, and M. Kučera (2009), Seasonal and interannual variability of the planktic foraminiferal flux in the vicinity of the Azores Current, *Deep Sea Res., Part I*, *56*(1), 107–124.
Takayanagi, Y., N. Niitsuma, and T. Sakai (1968), Wall microstructure of *Globorotalia truncatulinoides* (d'Orbigny), *Sci. Rep. Tohoku Univ.*, *40*, 141–170.
Thiede, J. (1971), Planktonische Foraminiferen in sedimenten vom ibero-marokkanischen Kontinentalrand, *Meteor Forschungsergeb. C*, *7*, 15–102.
Thierstein, H. R., K. R. Geitzenauer, B. Molfino, and N. J. Shackleton (1977), Global synchroneity of late Quaternary coccolith datum levels: Validation by oxygen isotopes, *Geology*, *5*(7), 400–404.
Tolderlund, D. S., and A. W. H. Be (1971), Seasonal distribution of planktonic foraminifera in the western North Atlantic, *Micropaleontology*, *17*(3), 297–329.
Ujiié, Y., and T. Asami (2013), Temperature is not responsible for left-right reversal in pelagic unicellular zooplanktons, *J. Zool.*, *293*, 16–24.
Ujiié, Y., and J. H. Lipps (2009), Cryptic diversity in planktic foraminifera in the northwest Pacific Ocean, *J. Foraminiferal Res.*, *39*(3), 145–154.
Ujiié, Y., T. de Garidel-Thoron, S. Watanabe, P. Wiebe, and C. de Vargas (2010), Coiling dimorphism within a genetic type of the planktonic foraminifer *Globorotalia truncatulinoides*, *Mar. Micropaleontol.*, *77*(3–4), 145–153.
Veldhuis, M. J. W., G. W. Kraay, and W. W. C. Gieskes (1993), Growth and fluorescence characteristics of ultraplankton on a north-south transect in the eastern North Atlantic, *Deep Sea Res., Part II*, *40*(1), 609–626.
Vergnaud-Grazzini, C. (1976), Non-equilibrium isotopic compositions of shells of planktonic foraminifera in the Mediterranean Sea, *Palaeogeogr. Palaeoclimatol. Palaeoecol.*, *20*(4), 263–276.
Vincent, E., and W. H. Berger (1981), Planktonic foraminifera and their use in palaeoceanography, in *The Sea*, edited by C. Emiliani, pp. 1025–1119, Wiley-Interscience, New York.
Westbroek, P., J. R. Young, and K. Linschooten (1989), Coccolith production (biomineralization) in the marine alga *Emiliania huxleyi*, *J. Protozool.*, *36*(4), 368–373.
Wiersma, A. P., and J. I. Jongma (2010), A role for icebergs in the 8.2 ka climate event, *Clim. Dyn.*, *35*(2–3), 535–549.
Wilke, I., H. Meggers, and T. Bickert (2009), Depth habitats and seasonal distributions of recent planktic foraminifers in the Canary Islands region (29 N) based on oxygen isotopes, *Deep Sea Res., Part I*, *56*(1), 89–106.
Worthington, L. V. (1968), Genesis and evolution of water masses, *Meteorol. Mongr.*, *8*(30), 63–67.
Zahn, R., J. Schönfeld, H. R. Kudrass, M. H. Park, H. Erlenkeuser, and P. Grootes (1997), Thermohaline instability in the North Atlantic during meltwater events: Stable isotope and ice-rafted detritus records from core SO75-26KL, Portuguese Margin, *Paleoceanography*, *12*(5), 696–710, doi:10.1029/97PA00581.